Technischer Bericht Nr. 95

Berichte über Beobachtungen an Längstwellen-Atmospherics
mit dem Atmospherics-Analysator
des Heinrich-Hertz-Instituts

Die Bearbeiter:

Dr. J. FRISIUS und Ing. G. HEYDT

Berlin
1968

Zusammenfassungen

Berichte über Beobachtungen an Längstwellen-Atmospherics
mit dem Atmospherics-Analysator des Heinrich-Hertz-
Institutes, Berlin-Charlottenburg, 1968.

I. A New Technique to Observe Spectral Parameters of the
VLF Radio Noise as Functions of the Azimuth

(Eine neuartige Technik zur Beobachtung spektraler
Parameter des atmosphärischen Störpegels im Längst=
wellenbereich unter Berücksichtigung der Einfallsrich=
tung)

Der Atmospherics-Analysator des Heinrich-Hertz-Institutes
gestattet die richtungsabhängige Bestimmung spektraler Pa=
rameter des atmosphärischen Funk-Störpegels im Längstwellen=
bereich. Die hierbei verwendeten technischen Prinzipien werden
in dieser Arbeit zusammengestellt.

Jedes Atmospheric erzeugt Spannungsimpulse in zwei gekreuzten
Rahmenantennen und einer vertikalen Stabantenne. Ein Peil=
gerät leitet aus den zwei Rahmenspannungen einen Gleich=
spannungsimpuls ab, dessen Höhe die Einfallsrichtung eindeu=
tig anzeigt. Die Stabantennenspannung kann wahlweise einer
der folgenden Analysator-Einheiten zugeführt werden:

1. Einem Schmalbandverstärker .; dieser liefert als Ausgangs=
spannung einen gleichgerichteten Impuls, dessen Maximal=
spannung der spektralen Amplitude des Eingangsimpulses
im Bereich der Verstärker-Durchlassfrequenz proportional
ist. Diese Frequenz kann beliebig im VLF-Bereich (5 bis
50 kHz) eingestellt werden.

2. Einem Verhältnismesser ; dieser liefert einen Ausgangs=
impuls, dessen Höhe eindeutig von dem Verhältnis zweier
spektraler Amplituden im Atmospherics-Spektrum abhängt.
Die Durchlassfrequenzen der in dieser Betriebsart ver=
wendeten zwei Schmalbandempfänger können beliebig im
VLF-Bereich eingestellt werden.

3. Einem Dispersions-Meßgerät ; die Ausgangsspannung dieses
Gerätes ist proportional der Gruppenlaufzeit-Differenz,
die zwischen dem Eintreffen zweier Spektralbereiche des
Atmospherics-Spektrum am Empfangsort verstreicht. Die
Mittenfrequenzen dieser Spektralbereiche können inner=
halb des unteren VLF-Bandes (4 bis 11 kHz) gewählt
werden.

Die Atmospherics können durch einen Oszillografen angezeigt
werden. Hierzu wird der vom Peilgerät gelieferte " Peilim=
puls" auf den Y-Verstärker, die Meßspannung auf den X-Ver=
stärker gegeben. Der Kathodenstrahl wird kurzzeitig hellge=
steuert, wenn der Meßspannungsimpuls seinen Spitzenwert
erreicht. Auf diese Weise erzeugt jedes Atmospheric einen
kurzzeitigen Lichtpunkt, dessen Lage auf dem Oszillografen=
schirm eindeutig von der Einfallsrichtung und der zu

messenden spektralen Größe abhängt. Photographiert man
den Schirm mit einer Belichtungszeit von einigen Minu=
ten, so erhält man Lichtpunkte von einigen tausend
Atmospherics, so daß die statistische Verteilung der
spektralen Größe über den Einfallsazimuth untersucht
werden kann. Eine programmierbare Schaltautomatik er=
möglicht die Durchführung langfristiger Meßprogramme.

II. Spectral Parameters of the VLF Radio Noise Obser= ved as Functions of the Azimuth

(Beobachtungen spektraler Parameter des atmosphä=
rischen Störpegels im Längstwellenbereich unter
Berücksichtigung der Einfallsrichtung)

Die Wirkungsweise eines neuartigen Atmospherics-Analy=
sators, welcher die Bestimmung spektraler Parameter des
Längstwellen-Funkstörpegels unter Berücksichtigung der
Einfallsrichtung gestattet, wird kurz erklärt. Die
physikalische Bedeutung der mit diesem Gerät meßbaren
spaktralen Größen wird anhand der Wellenleiter-Theorie
erläutert. Danach werden die Beobachtungen einer 4-wöchi=
gen Meßperiode so dargestellt, daß sie mit den Ergeb=
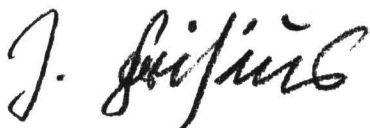nissen theoretischer Ausbreitungsberechnungen verglichen
werden können.

Berichte über Beobachtungen an Längstwellen-Atmospherics mit dem Atmospherics Analysator des Heinrich-Hertz-Instituts
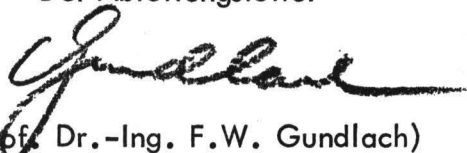
1. A New Technique to observe Spectral Parameters of the VLF Radio Noise as Functions of the Azimuth

2. Spectral Parameters of the VLF Radio Noise Observed as Functions of the Azimuth
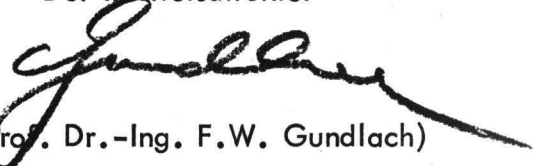
Die Bearbeiter

(Dr. J. Frisius)

(Ing. G. Heydt)

Der Abteilungsleiter

Der Institutsdirektor

(Prof. Dr.-Ing. F.W. Gundlach)

(Prof. Dr.-Ing. F.W. Gundlach)

Berlin-Charlottenburg, den 9. Februar 1968

A New Technique to observe Spectral
Parameters of the VLF Radio Noise as Functions of
the Azimuth

by

G. Heydt and J. Frisius
Heinrich-Hertz-Institut für Schwingungsforschung,
Berlin-Charlottenburg.

Abstract

The basic principles of a technique are described which
solve the problem of observing certain characteristics of
the VLF radio noise spectrum together with the apparent azi-
muth angle of arrival of the atmospherics. A direction finder
derives from the voltages induced by an atmospheric in a
crossed loop antenna system a single d-c pulse, the height of
which indicates the azimuth uniquely. From the pulse simul-
taneously induced in a vertical rod antenna d-c voltages can
be derived which measure the following spectral characteristics:

(a) The spectral amplitude of the atmospheric at a
    frequency to be chosen in the VLF range (5 to 50 kHz)
(b) the ratio between the spectral amplitudes at two
    frequencies to be chosen in the same range
(c) the difference between the group delay times of the
    spectral components at two frequencies, which can
    be chosen in the lower VLF range (4 to 11 kHz).

The technical realization of these ideas as developed at the Heinrich-Hertz-Institut, West-Berlin, uses an oscilloscope to monitor the atmospherics, the y-deflection for the azimuth and the x-deflection for measuring one of the characteristics listed above. Data of thousands of atmospherics can be obtained and stored by photographing the screen at an exposition time of several minutes. Automatic operation enables measurement programs to be easily carried out over long time periods. Examples of measurements are given and an appropriate presentation of the data is proposed.

1. Introduction

The usual methods of measuring the statistical parameters of the VLF radio noise do not permit to separate the contributions of specific direction sectors to the total received noise (URSI, 1962). This fact causes considerable difficulties for the interpretation of the measured data in terms of wave propagation theories. The present paper describes a new atmospherics analyzer which combines the finding of the direction of arrival of the atmospherics with the measurements of certain characteristics of their spectrum by a single measuring procedure. In this paper, the basic technical ideas will be outlined and the obtainable information on the atmospherics spectrum described. Results of observations using the new technique will be reported in a companion paper. A complete description of all technical details of the atmospheric analyzer has been given by Heydt (1967).

Fig. 1:
Block diagram of the atmospherics analyzer of the Heinrich-Hertz Institute
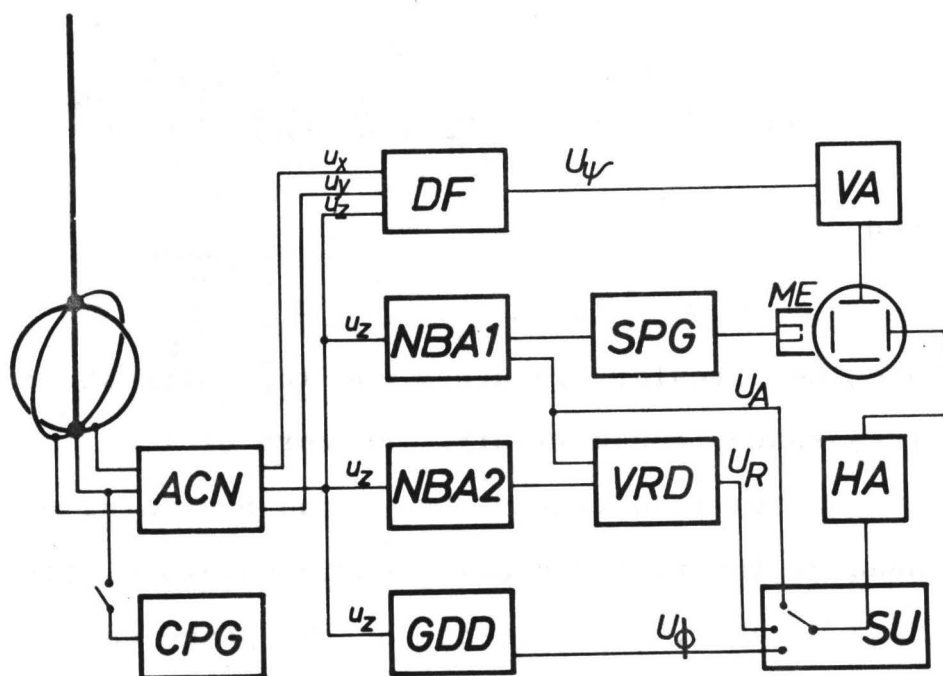
2. General Description

In this section the elements of the analyzer equipment and their responses to an incoming atmospheric pulse is surveyed. Further details on the elements are given in the subsequent sections.

2.1 Description of the Atmospheric

The vertical electric component E and the horizontal magnetic component H of the incoming signal is characterized by its amplitude spectrum $F(\omega)$ and its phase spectrum $\phi(\omega)$ as follows

$$E(t) = Z_c H(t) = \int_{-\infty}^{+\infty} F(\omega) e^{j\phi(\omega)} e^{j\omega t} d\omega \qquad (1a)$$

or in real form

$$E(t) = Z_0 H(t) = \int_0^{\infty} 2 F(\omega) \cos(\omega t + \phi(\omega)) d\omega \qquad (1b)$$

where

$$F(\omega) e^{j\phi(\omega)} = \frac{1}{2\pi} \int_C^{\infty} E(t) e^{-j\omega t} dt \qquad (1c)$$

and

$$\omega = 2\pi f \quad , \quad Z_c = \sqrt{\frac{\mu_c}{\varepsilon_c}} = 377 \, \Omega$$

are the circular frequency and the intrinsic impedance of the free space, respectively. The zero of the time axis in (1c) is defined by the beginning of the oscillatory head of the received atmospheric waveform. Its exact position has, however, no influence on the phase spectrum characteristic, the measurement of which is described below.

In denoting the apparent angle ψ of arrival of the atmospheric, we follow the common use to identify the direction $\psi = 0$ with north and the y-axis, the direction $\psi = 90^{\circ}$ with east and the x-axis of a cartesian coordinate system, that has its origin at the observing point.

2.2 The Direction Finder

The atmospheric pulse induces oscillatory voltage pulses in two crossed loops and a vertical rod of a conventional direction finding antenna system (fig. 1). The output voltages u_x, u_y, and u_z of the antenna coupling network (ACN in fig. 1) are fed into the direction finding system DF, which is operating at a narrow frequency band around 11 kHz. The direction finder derives a d-c pulse with a pulse height U_ψ, which is proportional to the azimuth ψ of arrival of the atmospheric. This "bearing pulse" is led to the vertical amplifier VA of an oscilloscope system. Thus, the direction is uniquely indicated by the vertical deflection of the cathode ray, and the horizontal deflection can be used to give an information on any characteristic of the atmospherics spectrum.

2.3 Spectral Amplitude Measurements

The horizontal deflection can for example be used to measure the spectral amplitude $F(\omega)$ of the atmospheric at an arbitrarily chosen frequency of the VLF range (5 to 50 kHz). To this end, the vertical rod voltage u_z is fed into a tunable narrow band amplifier denoted NBA1 in fig. 1. This amplifier produces a rectified pulse U_A, that has a peak voltage U, proportional to the spectral amplitude of the atmospheric at the

resonance frequency of the amplifier. The pulse U_A is fed

    a) into the horizontal amplifier HA of the oscillo-
       scope

    b) into a differentiation network (SPG) which generates
       a sensitizing pulse of short duration and large
       amplitude at that moment when the pulse U_A passes
       through its maximum value U.

The "sensitizing pulse" is led to the modulator electrode ME
of the oscilloscope to control the brightness of the cathode
ray. Thus, the atmospheric appears only for a short moment on
the oscilloscope screen at a position, which is uniquely re-
lated to its direction and spectral amplitude.

A measurement of the distribution of the atmospherics with
respect to both amplitude and direction of arrival can be per-
formed by photographing the oscilloscope screen with an expo-
sition time of several minutes. The photo contains light spots
produced by some thousands of atmospherics and the distribution
can be obtained by counting. Examples of such photographs are
shown below.

2.4 Spectral Amplitude Ratios
and Group Delay Time Differences

A second narrowband amplifier (NBA2) measures the atmo-
spherics spectral amplitude at another frequency. The output
voltages of the two amplifiers NBA1 and NBA2 are fed into a
voltage ratio detector (VRD) to give a d-c pulse U_R. The pulse
height of U_R is a known function of the ratio between the
spectral amplitudes at the resonance frequencies of the two
amplifiers. Replacing the pulse U_A of the preceding section by

U_R, a measurement of the spectral amplitude ratio can be carried out in the same way as described above.

A third mode of operation of the analyzer enables measurements of the dispersion of the pulse spectrum. The group delay time difference unit (GDD) derives from every incoming atmospheric a rectified voltage pulse $U_\emptyset$. Here, the pulse height of $U_\emptyset$ is proportional to the difference Δt_g between the group delay times of the spectral components at two frequencies that can be chosen in the lower VLF range (5 to 10 kHz).

The group delay time difference is related to the phase spectrum of the atmospheric. The latter is usually determined by numerical Fourier analysis of atmospheric wave forms. The new atmospherics analyzer provides related informations in the same simply evaluable form as the distributions of spectral amplitudes and amplitude ratios.

2.5 Automatic Operation and Calibration

The constancy and reliability of all electronic elements of the device can easily be checked by connecting the antenna input with a calibration pulse generator (CPG). This unit produces pulses which are very similar to real atmospherics, but have a spectrum well-known with respect to both amplitude and phase.

The equipment can be operated either by hand switching using a polaroid camera or by automatic switching using an automatic camera recorder. During automatic operation, all required characteristics of the measurement, e.g. exposition

times, mode of operation, operation frequency, antenna input
attenuation etc., are selected by a programmable switching
unit (SU). This unit enables a series of six measurements of
different spectral characteristics to be regularly repeated.

Regular stability tests can also be carried out automati-
cally. Thus, measuring programmes over large time periods can
be carried out without the steady presence of observing per-
sonnel being necessary.

Fig. 2a: Configuration of the
magnetic vector $\underline{H}(t)$ and
the wave normal for an in-
cident plane wave,

2b: Components of an ellip-
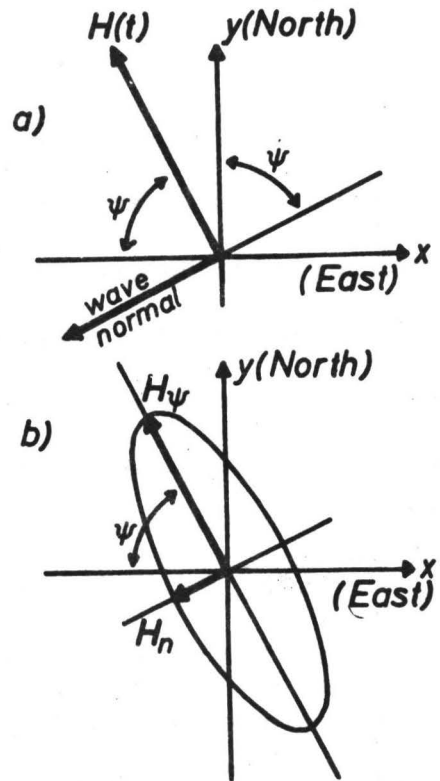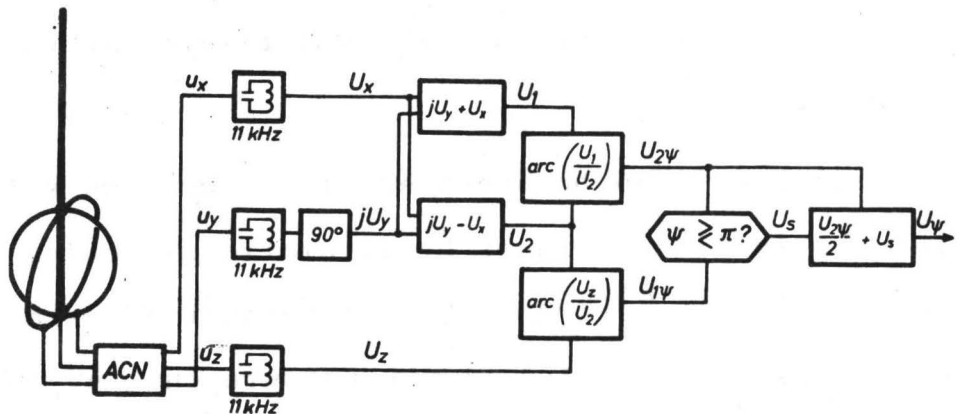tically polarized magnetic
vector

Fig. 3: Block diagram of the
direction finder system

3. Basic Principles of the Direction Finder System

The main problem in developing the atmospherics analyzer was unique indication of the direction of arrival by a single d-c voltage pulse. The first simple solution of this problem was presented by Heydt (1964). The final performance of the analyzer uses a considerably more reliable principle of deriving a "bearing pulse", that is described in this section.

3.1 The Derivation of Voltages
Indicating the Direction of Arrival.

The incoming electromagnetic field is assumed to be a plane wave with a linearly polarized magnetic vector, parallel to the surface of the earth. The effect of an elliptically polarized magnetic vector on the system will be discussed in subsection 3.3.

The configuration of the magnetic vector and the propagation direction is shown by fig. 2a. The magnetic field induces the voltage u_x in the loop parallel to the xz-plane, the voltage u_y in the loop parallel to the yz-plane, and the voltage u_z in the vertical rod antenna, where

$$u_x = k_H \frac{\partial H_y(t)}{\partial t} = k_H \frac{\partial H(t)}{\partial t} \sin \psi$$

$$u_y = k_H \frac{\partial H_x(t)}{\partial t} = - k_H \frac{\partial H(t)}{\partial t} \cos \psi \qquad (2)$$

$$u_z = k_z E(t) = k_z Z_0 H(t)$$

Here, k_H and k_z are antenna sensitivity factors which can in general neither be assumed to be real nor constant with time, i.e. independent of meteorological and geographical influences.

The voltages u_x, u_y, and u_z are fed into three identical narrowband amplifiers, tuned to the carrier frequency ω_c (see fig. 3).

The output voltages are oscillatory pulses which can be written in complex form

$$U_x(t) = k_H V(t) j\omega_c \frac{F(\omega_c)}{Z_o} e^{j(\omega_c t + \phi(\omega_c))} \sin\psi$$

$$U_y(t) = -k_H V(t) j\omega_c \frac{F(\omega_c)}{Z_o} e^{j(\omega_c t + \phi(\omega_c))} \cos\psi \qquad (3a)$$

$$U_z(t) = k_z V(t) F(\omega_c) e^{j(\omega_c t + \phi(\omega_c))}$$

Here, V(t) describes a d-c pulse, the shape of which depends on the construction of the amplifier, only. For a two stage resonance amplifier, e.g., it can be shown (Heydt, 1967 p. 30 ff.) that V(t) has the form

$$V(t) = V_o \frac{t}{\mathcal{T}} e^{-\frac{t}{\mathcal{T}}} \qquad (3b)$$

where V_o is an amplification constant and $\mathcal{T}$ a time constant. Equation (3b) usefully describes also the rectified impulse response of other narrowband amplifier types.

One of the loop excited voltages, e.g. U_y, passes a phase delay network, shifting its phase by 90°. Thus, the phase shifted voltage may be written as jU_y. Adding $+U_x$ or $-U_x$ to jU_y gives the following two voltages U_1 and U_2:

$$U_1(t) = jU_y + U_x = k_H V(t) \omega_c \frac{F(\omega_c)}{Z_o} e^{j(\omega_c t + \phi(\omega_c))} e^{j\psi}$$

$$U_2(t) = jU_y - U_x = k_H V(t) \omega_c \frac{F(\omega_c)}{Z_o} e^{j(\omega_c t + \phi(\omega_c))} e^{-j\psi} \qquad (4)$$

The phase difference between U_1 and U_2 is independent of the spectral amplitude of the atmospheric at the frequency ω_c:

$$\frac{U_1(t)}{U_2(t)} = e^{j2\psi} \qquad (5)$$

It can easily be measured by a phase detector unit, which gives a d-c pulse with a pulse height $U_2\psi$, proportional to twice the azimuth angle.

The phase difference between U_z and U_1 or U_2 is independent of the spectral amplitude and equal to the azimuth angle, provided k_z and k_H are real:

$$\frac{U_z(t)}{U_2(t)} = \frac{k_z Z_0}{k_H \omega_c} e^{j\psi} \quad , \quad \frac{U_z(t)}{U_1(t)} = \frac{k_z Z_0}{k_H \omega_c} e^{-j\psi} \qquad (6)$$

A phase detector fed by U_z and U_1 or U_2 gives d-c output voltage $U_1\psi$ proportional to the azimuth angle.

The voltage $U_1\psi$ has the advantage of easily being derived and uniquely giving the azimuth. It is, however, affected by the unknown phase angle γ of the antenna sensitivity ratio k_z/k_H. The voltage $U_2\psi$ is free from such unknown influences, but does not uniquely give the direction. Two bearing directions which differ by $180°$ give the same value of $U_2\psi$. Therefore, in previous publications (Volland, 1964), only the derivation of $U_1\psi$ has been described. The atmospherics digital data collection system, reported most recently by Grubb (1967) uses also $U_1\psi$. It is, however, possible to remove the ambiguity of $U_2\psi$ by means of a logical circuit, that will be described in the next subsection. This circuit derives a voltage U_s depending upon ψ as follows:

$$U_s = \begin{cases} 0 & \text{for } 0° \leq \psi < 180° \\ U_\pi & \text{for } 180° \leq \psi < 360° \end{cases} \qquad (7)$$

Here, U_π is half of that value of $U_{2\psi}$ that indicates the angles $\psi = \pi$ or $\psi = 2\pi$. The voltage U_s is not influenced by the unknown complex antenna sensitivity ratio k_Z/k_H, provided its phase angle γ does not exceed certain limiting values $\pm \gamma_{lim}$, that can be chosen up to $\pm 60^\circ$, say. The voltage

$$U_\psi = \frac{U_{2\psi}}{2} + U_s \tag{8}$$

indicates therefore the direction ψ uniquely without being influenced by any antenna factors.

3.2 The Logical Circuit Providing
Unique Direction Indication

Subtracting the half of $U_{2\psi}$ from $U_{1\psi}$ we get the test voltage U_t

$$U_t = U_{1\psi} - \frac{1}{2} U_{2\psi} \tag{9}$$

In case of $\gamma = 0$, U_t is the same function of ψ as U_s defined by (7) (see fig. 4 a and b). In case of $\gamma \neq 0$, however, $U_{1\psi}$ plotted as a function of ψ, is shifted relatively to $U_{2\psi}$ as shown by fig. 4c and e. The test voltage $U_t(\psi)$ shows in any case a jump of $+U_\pi$ at $\psi = \pi$, for positive γ a jump of $-2U_\pi$ at $\psi = 2\pi - \gamma$, and for negative γ at $\psi = |\gamma|$. We may assume that γ does not exceed the limits $\pm \gamma_{lim}$, where γ_{lim} is allowed to assume values up to 60°, say. Figure 4 shows, that in this case U_t is defined by table 1.

If the angle γ is limited as mentioned above, the function U_t assumes for the different ranges of the argument ψ well distinguishable values, which allow to decide whether or not

$\gamma > 0$		$\gamma < 0$	
ψ	U_t	ψ	U_t
$0\ldots\pi$	$U_\pi\,\gamma/\pi$	$0\ldots|\gamma|$	$U_\pi(2\pi-|\gamma|)/\pi$
$\pi\ldots 2\pi-\gamma$	$U_\pi(\pi+\gamma)/\pi$	$|\gamma|\ldots\pi$	$-U_\pi|\gamma|/\pi$
$2\pi-\gamma\ldots 2\pi$	$-U_\pi(\pi-\gamma)/\pi$	$\pi\ldots 2\pi$	$U_\pi(\pi-|\gamma|)/\pi$

Table 1: Values of the test voltage U_t for positive and negative values of γ and different ranges of the azimuth ψ .

Fig. 4a – f:
The voltages $U_{1\psi}$, $U_{2\psi}$, and U_t as functions of the azimuth ψ for $\gamma = 0$, $\gamma > 0$, and $\gamma < 0$.

4g: Logical scheme for the determination of U_s.
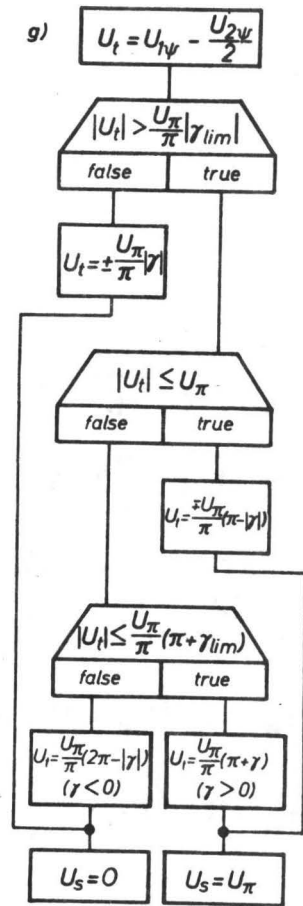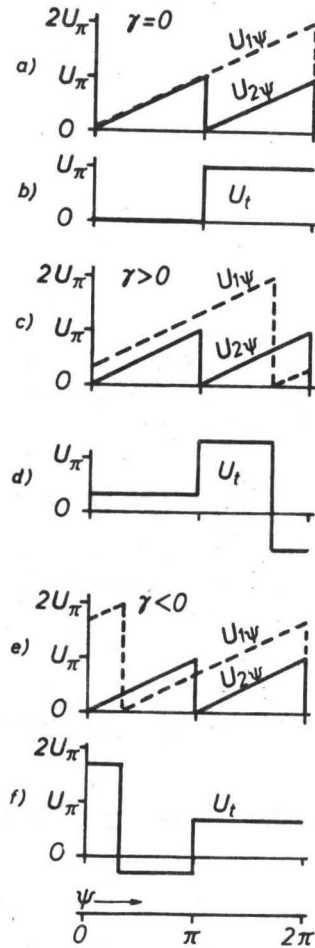
ψ is greater than π, i.e., whether U_s must have the value U_π or zero. The decision is carried out by a circuit, which realizes the logical scheme of fig. 4g.

3.3 The Response of the Direction Finder to an Elliptically Polarized Magnetic Vector

It is well-known, that on the oscilloscope screen of conventional cathode ray direction finders many atmospherics give an elliptic trace. This indicates that the spectral component of the magnetic field in general must be described by an elliptic oscillation.

The meaning of the symbol ψ is now restricted to be the angle between the major axis of the oscillation ellipse of the magnetic field and the negative x-axis (see fig. 2b). The field is now composed by two components H_ψ and H_n parallel and normal respectively to the major axis direction. The loop antenna voltages are now

$$u_x = k_H \frac{\partial H_y}{\partial t} = k_H \left(\frac{\partial H_\psi}{\partial t} \sin\psi - \frac{\partial H_n}{\partial t} \cos\psi \right)$$
$$u_y = k_H \frac{\partial H_x}{\partial t} = -k_H \left(\frac{\partial H_\psi}{\partial t} \cos\psi + \frac{\partial H_n}{\partial t} \sin\psi \right)$$

(10)

The spectral components of H_ψ and H_n near the carrier frequency ω_c may be written as

$$\Delta H_\psi = h_\psi(\omega_c) \cos\omega_c t \, \Delta\omega = Re\left(h_\psi e^{j\omega_c t} \Delta\omega \right)$$
$$\Delta H_n = h_n(\omega_c) \sin\omega_c t \, \Delta\omega = Re\left(-j\alpha \, h_\psi e^{j\omega_c t} \Delta\omega \right)$$

(11)

Here, the axis ratio

$$\alpha = \alpha(\omega_c) = \frac{h_n(\omega_c)}{h_\psi(\omega_c)}$$

(12)

depends, of course, upon the choice of ω_c, and $\Delta\omega$ may be imagined to be the bandwidth of the narrow band amplifiers.

It can easily be seen that the amplifier response can be written in the form

$$U_x(t) = j\omega_c K(t)(\sin\psi + j\alpha\cos\psi)$$

$$U_y(t) = -j\omega_c K(t)(\cos\psi - j\alpha\sin\psi)$$

(13)

The function $K(t)$ describes an oscillatory pulse similar to that described by (3a) and (3b). The voltages U_1 and U_2 of (4) become now

$$U_1 = jU_y + U_x = \omega_c K(t)[(\cos\psi + j\sin\psi) - \alpha(\cos\psi + j\sin\psi)]$$

$$U_2 = jU_y - U_x = \omega_c K(t)[(\cos\psi - j\sin\psi) + \alpha(\cos\psi - j\sin\psi)]$$

(14)

The effect of the elliptic polarization therefore is to decrease U_1 and to increase U_2. The phase difference between U_1 and U_2 is again twice the angle ψ:

$$\frac{U_1}{U_2} = \frac{1-\alpha}{1+\alpha}e^{j2\psi}$$

(15)

We conclude, that the direction finder generally indicates the larger axis angle ψ, defined at the beginning of this sub-section. Equation (15) reveals the considerable advantages of using only the loop antenna voltages for the direction determination. Amplitude and phase of the ratio U_1/U_2 only depend upon the ellipticity α or the axis direction ψ, respectively. In the atmospherics analyzer, use has been made only of the phase measurement, but it would be an easy matter to provide a determination of the ellipticity by measuring the amplitude of the ratio U_1/U_2.

4. Principles of the Spectral Amplitude
and Group Delay Time Difference Measurements

If the problem of the direction finding is solved, the measurement of the spectral amplitude as described in section 2.3 is not difficult and needs no further explanation. Amplitude ratios can be measured most exactly be means of modern operational amplifiers, and, indeed, the VRD of one of the four existing analyzers consists of such elements. In this paper, however, an inexpensive and very simply feasible extension of the principle described in section 3.1 for the ratio measurement is given. Both amplitude ratios and group delay time differences are converted into phase differences between a-c voltages in the low frequency range. This considerably simplifies the technique, because for both measurements the same type of phase detector can be used.

4.1 Spectral Amplitude Ratios

The vertical rod antenna voltage u_z is fed into the narrow-band amplifiers NBA1 and NBA2, which are tuned to the frequencies ω_1 and ω_2 (fig. 5, upper part). The rectified output voltages are

$$U_{A1} = k_z V(t) F(\omega_1) \quad , \quad U_{A2} = k_z V(t) F(\omega_2) \tag{16}$$

The amplifier construction (Heydt, 1967) ensures, that the function $V(t)$ is exactly the same for both amplifiers. The d-c pulse U_{A2} is used to modulate an a-c voltage of the carrier frequency ω_c (note, that the meaning of symbols for auxiliary quantities, e.g. ω_c, U_1, U_2, etc. may change from subsection to subsection). The pulse U_{A1} modulates an a-c voltage of the

same frequency, which is phase shifted by 90° relative to the first pulse. The resulting oscillatory pulses are written in complex form

$$U_1 = j U_{A1} e^{j\omega_c t} \quad , \quad U_2 = U_{A2} e^{j\omega_c t} \tag{17}$$

Adding U_2 to $+U_1$ or $-U_1$ gives the voltages U_I and U_{II}:

$$U_I = U_1 + U_2 \quad , \quad U_{II} = -U_1 + U_2 \tag{18}$$

and it can easily be seen that the phase difference between U_I and U_{II} is

$$arc\left(\frac{U_I}{U_{II}}\right) = 2 \arctan\left(\frac{U_{A1}}{U_{A2}}\right) = 2\arctan\left(\frac{F(\omega_1)}{F(\omega_2)}\right) \tag{19}$$

Thus, if the voltages U_I and U_{II} are fed into the phase detector unit, the output voltage U_R is proportional to twice the arcus-tangens of the spectral amplitude ratio between the frequencies ω_1 and ω_2.

Fig. 5:
Block diagram of the spectral amplitude ratio and group delay time difference measurement
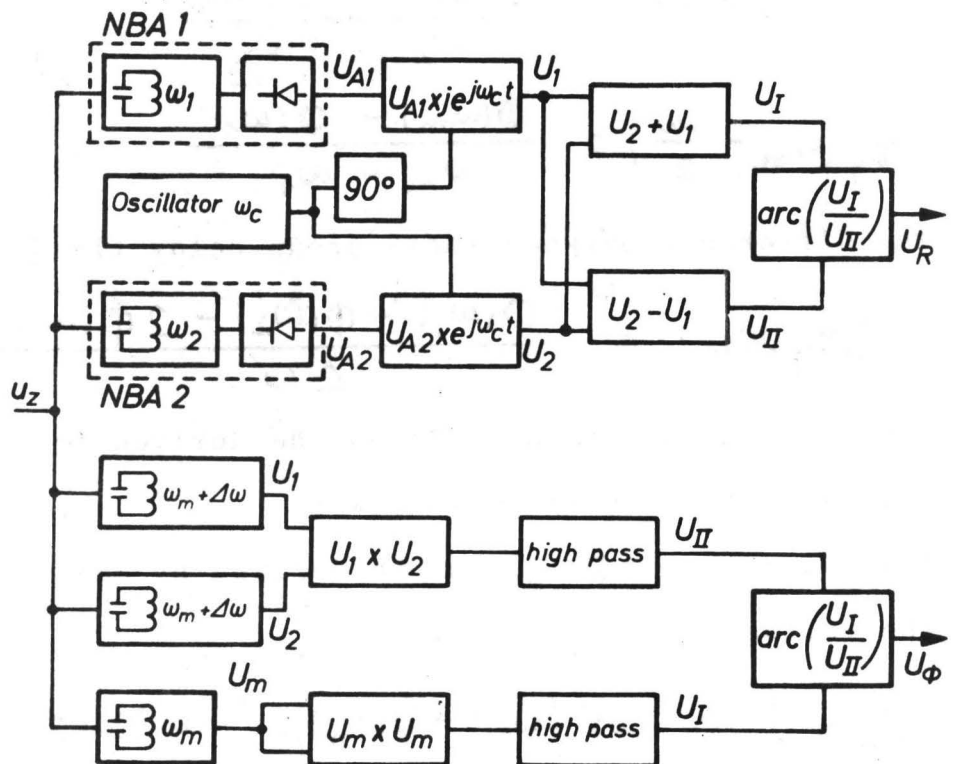
4.2 Spectral Group Delay Time Differences

The vertical antenna voltage, written here in real form

$$u_z = k_z E(t) = 2k_z \int_0^\infty F(\omega) \cos(\omega t + \phi(\omega)) d\omega \qquad (1b)$$

is fed into three resonance amplifiers tuned to the respective frequencies

$$\omega_1 = \omega_m - \Delta\omega, \qquad \omega_m, \qquad \omega_2 = \omega_m + \Delta\omega \qquad (20)$$

which range from 4 to 11 kHz.

The amplifier output voltages are oscillatory pulses

$$U_1 = V(t) F(\omega_1) \cos(\omega_1 t + \phi(\omega_1))$$

$$U_2 = V(t) F(\omega_2) \cos(\omega_2 t + \phi(\omega_2)) \qquad (21)$$

$$U_m = V(t) F(\omega_m) \cos(\omega_m t + \phi(\omega_m))$$

The group delay times at the frequencies $\omega_m + \Delta\omega/2$ and $\omega_m - \Delta\omega/2$ can be approximated by the following difference quotients

$$t_g\left(\omega_m + \frac{\Delta\omega}{2}\right) = \frac{\phi(\omega_2) - \phi(\omega_m)}{\omega_2 - \omega_m}$$

$$t_g\left(\omega_m - \frac{\Delta\omega}{2}\right) = \frac{\phi(\omega_m) - \phi(\omega_1)}{\omega_m - \omega_1} \qquad (22)$$

The difference between these group delay times is

$$\Delta t_g(\omega_m) = \frac{\phi(\omega_1) + \phi(\omega_2) - 2\phi(\omega_m)}{\Delta\omega} \qquad (23)$$

The right hand term of (23) can be derived from the amplifier output voltages (21) as follows:

The phase term $2\phi(\omega_m)$ can be derived by multiplicative mixing the voltage U_m with itself:

$$U_m \times U_m \sim \cos^2(\omega_m t + \phi(\omega_m)) = \frac{1}{2}\left[\cos(2\omega_m t + 2\phi(\omega_m)) + 1\right]$$

The constant term is removed by a high pass filter, the output of which is

$$U_I \sim \cos(2\omega_m t + 2\phi(\omega_m)) \tag{24}$$

The term $\phi(\omega_1) + \phi(\omega_2)$ is derived by multiplicative mixing the voltages U_1 and U_2:

$$U_1 \times U_2 \sim \cos\left[(\omega_1+\omega_2)t + \phi(\omega_1) + \phi(\omega_2)\right] + \cos\left[(\omega_2-\omega_1)t + \phi(\omega_2) - \phi(\omega_1)\right]$$

The lower frequency term is removed by a high pass filter, which supplies the voltage

$$U_{II} \sim \cos\left[2\omega_m t + \phi(\omega_1) + \phi(\omega_2)\right] \tag{25}$$

The phase difference between the voltages U_I and U_{II} is now

$$\Delta\phi = \phi(\omega_1) + \phi(\omega_2) - 2\phi(\omega_m) \tag{26}$$

The phase detector unit supplies therefore an output voltage

$$U_\phi \sim \Delta t_g \Delta\omega \tag{27}$$

proportional to the product from the known frequency distance $\Delta\omega$ and the group delay time difference between the spectral components at the frequencies $\omega_m + \Delta\omega/2$ and $\omega_m - \Delta\omega/2$.
This principle of group delay time measurement has been described firstly by Heydt (1965).

5. Remarks on Technical Realization

Details on the technical realization of the ideas outlined in the preceding sections are out of the scope of this paper and can be found elsewhere (Heydt, 1967). Only a few remarks concerning the analyzers of the Heinrich-Hertz-Institut should complete this report.

The explanations of sections 3 and 4 are simplified by use of the well-known impulse response of simple resonance amplifiers. In the performed equipments, however, amplifiers of the superheterodyne type have been used.

Pertinent use of transistorized circuits enable the equipments to be kept small. The size (without oscilloscopes) is $105 \times 105 \times 35$ cm (see fig. 6), and the weight about 120 kg. No external temperature and a-c power stabilization is necessary for contineous reliable operation. Thus, the apparatus is easily transportable.

All amplifier and phase detector output voltages are normalized to have the same maximal value 4 V. Thus, later developments for digitalizing the output voltages are prepared. A survey on some important technical data is given in table 2.

The reliability and stability of all electronic elements has been tested by an observation period from fall, 1966, to December 1967. During this time, four analyzers, two in Berlin, and two at observation stations far distant from each other in West Germany, had been contineously operating. Some 200 000 photos have been obtained, examples of which are shown below. Observational results are subject of a companion paper. In this paper it is only interesting, that no serious failure has occured during the mentioned period.
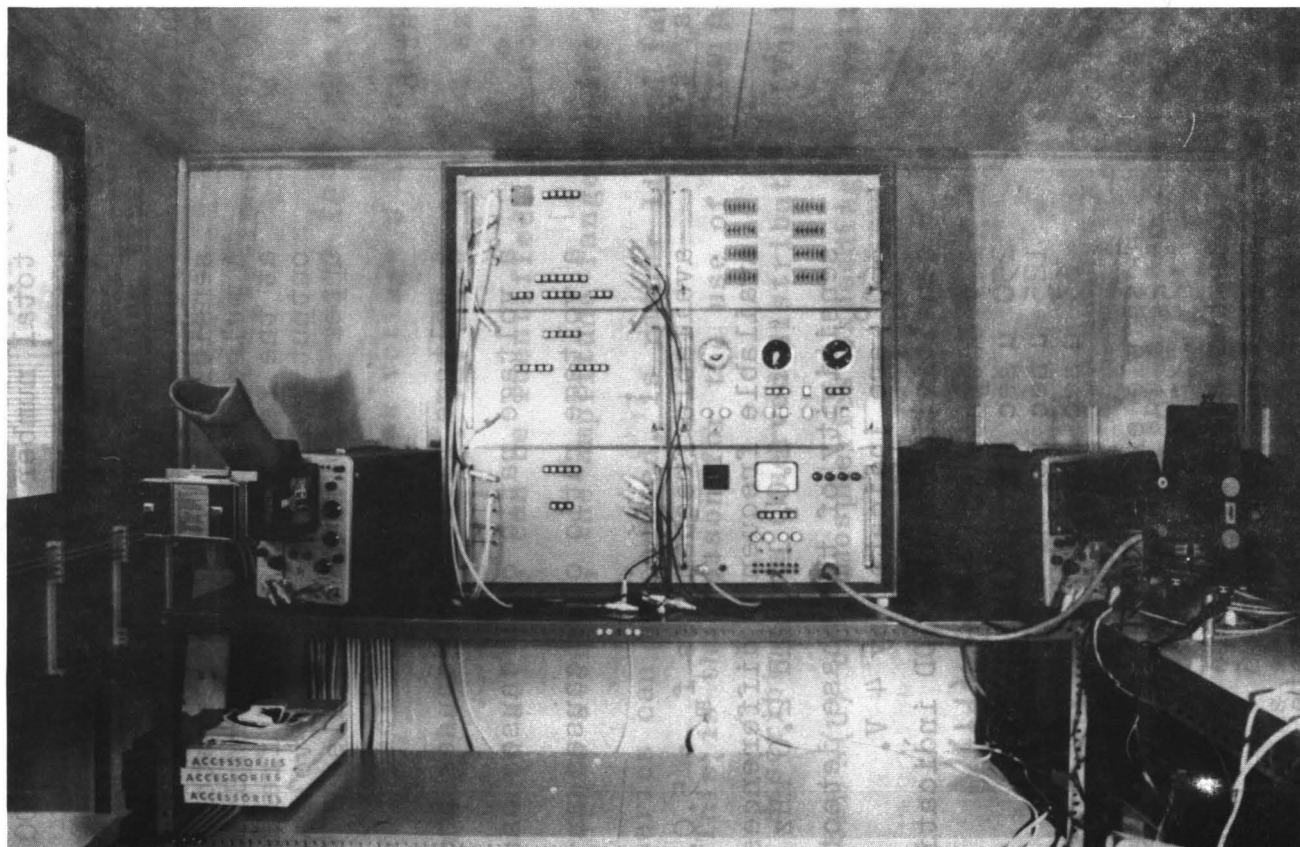
Fig. 6: Front view of the atmospherics anlyzer.

Vertical antenna :	length: 4.8 m diameter: 10 mm $h_{eff} \approx$ 1.4 m
Loop antennas :	ferrit core antennas length : 4 rods with a length of 240 mm diameter : 12 mm total number of wirings : 4000
Input attenuator :	0, 6, 12, 18, 24 dB
Narrow band amplifiers	Frequency range:5 to 50 kHz, bandwidth $\approx$ 200 Hz; sensitivity (input attenuator 0 dB) : A pulse with a spectral amplitude of 10 μV/Hz at the receiver's midband frequency causes a d.c. output pulse with a peak voltage of 2 V. upper limit of output pulse : 4,5 V
Voltage ratio detector:	a voltage ratio of 0 causes an output voltage of 0 V a voltage ratio of 1 causes an output voltage of 1 V a voltage ratio of ∞ causes an output voltage of 2 V
Group delay time difference unit:	available frequencies f_m : 5.0, 6.0, 7.0, 8.0 and 10.0 kHz available frequency differences Δf : 1.0, 1.4 and 2.0 kHz sensitivity of the phase detector : 360° are indicated by 4 V. sensitivity of the GDD indication : 1 V output voltage indicates 250 u sec for Δf = 1.0 Hz 125 u sec for Δf = 1.4 kHz 63 μ sec for Δf = 2.0 kHz
Programmable switching unit:	possible exposition time per measurement: 2,5 , 5.0 and 10.0 minutes. number of programmable measurements per measurements series: 6 possible repetition rate of the measurements series : 1/30 min, 1/60 min, 1/120 min.

Table 2 : Technical data of the atmospherics analyzer
of the Heinrich-Hertz-Institut

6. Examples of Measurements

In figure 7 a compact survey is given on the information
obtainable by the atmospherics analyzer. To the left, photos
of the three types described in section 2.2 to 2.4 are shown,
to the right, results are plotted which can be obtained by
evaluating several photos of corresponding type.

6.1 Spectral Amplitude Distributions

The distribution of the spectral component (at 9 kHz in this
example) with respect to output peak voltage U and azimuth ψ is
measured by photos as shown by fig. 7a. Here, several azimuth
sectors of enhanced activity can be identified. As a consequence
of the photographic storing, the amplitude range, inside of which
single atmospherics can be counted, is rather limited (about
10 to 20 dB). This is the reason for the use of the following
simple law for describing the observed distribution (Volland,
1964): The number N(U) of atmospherics exceeding the voltage U
is approx.

$$N(U) = N_o\, e^{-\frac{U}{U_m}} \tag{28}$$

This law involves only two unknown, the number N_o, characterizing
roughly the pulse frequency of the source, and the "average" vol-
tage U_m characterizing the decrease of the distribution with in-
creasing threshold. As soon as the photographic storing is re-
placed by digital storing methods, the distribution can be tried
to be described by more realistic laws. The number of atmos-
pherics exceeding the maximum voltage U_1, measurable by the oscil-
loscope (4V, see section 5) can be found by a second photo with
enhanced antenna input attenuation. U_m is given in dB relative
to the limiting voltage U_1 of the first photo.

6.2 Spectral Amplitude Ratio and
Group Delay Time Difference Distributions

A measurement of spectral amplitude ratios between 8 and
6 kHz is shown by fig. 7c. The direction sectors of enhanced
activity are characterized by certain values of the spectral
amplitude ratio, around which the atmospherics appear to be
clustered within rather narrow limits. There are many cases
where different sources with identical azimuth can be distin-
guished by an amplitude ratio measurement photo. Further mea-
surements of this kind have been carried out using the frequen-
cy pairs 8,9 kHz, 8,11 kHz, 8,13 kHz, and 13,21 kHz. Thus, the
part of the spectrum containing the well-known maximum at abt.
10 to 18 kHz can be constructed as shown by fig. 7d for two
azimuths.

Group delay time difference measurements give photos as fig.7e,
showing an example with the middle frequency f_m = 8 kHz and the
frequency distance Δf = 2 kHz. Again, single sources are in-
dicated by characteristical clusters, the center of which can
easily be read of from the photo. It is suggested by experience
that this type of measurement is especially suited for distin-
guishing different atmospherics sources with the same azimuth.
A series of three group delay time difference measurements gives
a part of the "dispersion spectrum" as shown by fig. 7f. Here,
the abscissa is divided by a f^{-3}-scale, because the simple flat
earth approximation of the VLF wave guide theory predicts pro-
portionality between the group delay time difference and f^{-3}.
This proportionality can be observed so frequently, that the
presentation employed by fig. 7f is believed to be useful as a
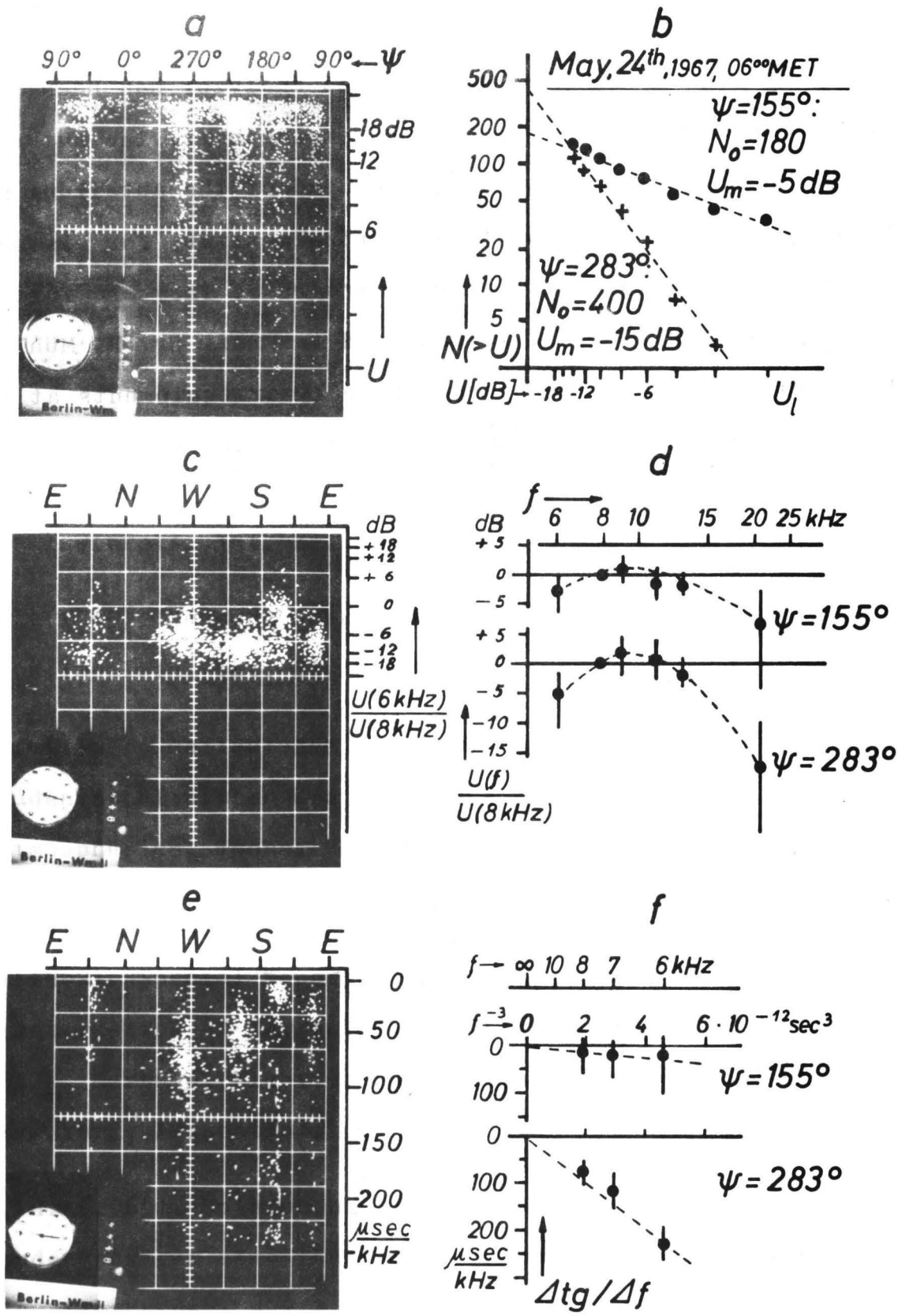standard.

Fig. 7, a-f: Examples of atmospherics analyzer photos
and evaluations (commented by section 6).

Acknowledgements

References

Grubb, R. N. (1967). A Digital Data Collection System for
Transient Waveforms in the 1 to 100 kHz Band and its
Application to the Study of Atmospherics.
Conference on MF, LF, and VLF Radio Propagation,
8th – 10th Nov., I.E.E., London.
Conference publication,p. 339 – 345.

Heydt, G. (1964). Messung der Verteilung der spektralen Ampli-
tuden von Atmospherics unter Berücksichtigung des Ein-
fallswinkels. Int. El. Rdsch. 18,   680 – 682.

Heydt, G. (1965). Messung spektraler Gruppenlaufzeitdifferenzen
von Impulsen. Int. El. Rdsch. 19, 426 – 428.

Heydt, G. (1967). Peilanlagen zur Messung von spektralen Ampli-
tudenverhältnissen und Gruppenlaufzeitdifferenzen von
Atmospherics. Techn. Ber. Nr. 90 des Heinrich-Hertz-In-
stitutes für Schwingungsforschung, Berlin-Charlottenburg.

URSI   (1962). Special Report No. 7 on The Measurement of Cha-
racteristics of Terrestrial Radio Noise. Gen. Ed.:
E. H. Herbays.(Elsevier Publ. Comp. Amsterdam, London,
New York, Princeton).

Volland, H. (1964). Untersuchungen über das statistische Ampli-
tudenspektrum atmosphärischer Störungen von einzelnen
Gewitterherden. N.T.Z. 17, 407 – 412.

Spectral Parameters of the VLF

Radio Noise Observed as Functions of the Azimuth

by

J. Frisius and G. Heydt

Heinrich-Hertz-Institut für Schwingungsforschung

Berlin-Charlottenburg

Abstract

The actions of a new atmospherics analyzer, which determines
for every incoming atmospheric the apparent angle of arrival
together with certain characteristics of the VLF spectrum,
are briefly explained. Then the physical significance of the
observable spectral quantities are considered by use of a sim-
plified version of the VLF wave guide mode theory. Finally,
spectral observations of a four weeks' period are presented
in such a way, that the influence of daytime and azimuth are
evident and comparison with theoretical propagation compu-
tations is enabled.

1. Introduction

The observations reported in the following communication
have been carried out by means of a new type of atmospherics
analyzer (Heydt, 1967). This equipment realizes technical ideas
which are dealt with by a companion paper (Heydt and Frisius,
1968). It combines the finding of the direction of arrival of
an incoming atmospheric pulse with the measurement of certain
of its spectral characteristics. Data of several thousands of
atmospherics can be collected during a few minutes and the di-
stribution of their spectral characteristics with respect to
the azimuth can be studied. It has been experienced (Heydt,
Frisius, Volland, and Harth, 1967) that the spectral quantities
observable by the new analyzer are characteristic functions of
both azimuth and time of day. A concise description of these re-
lations and a consideration of their physical significance is
the subject of this paper.

2. The Actions of the Atmospherics Analyzer

Let us consider an atmospheric, produced by an atmospherics source at the distance φ, observed at the apparent angle of incidence ψ. The vertical electric field strength E_z of the signal is described by its amplitude spectrum $F(\omega, \varphi)$ and phase spectrum $\phi(\omega, \varphi)$ as follows

$$E_z(\varphi, t) = \int_{-\infty}^{+\infty} F(\omega, \varphi) e^{j\phi(\omega, \varphi)} e^{j\omega t} \, d\omega \tag{1a}$$

or in real form

$$E_z(\varphi, t) = \int_{0}^{\infty} 2 F(\omega, \varphi) \cos(\omega t + \phi(\omega, \varphi)) \, d\omega \tag{1b}$$

where

$$F(\omega, \varphi) e^{j\phi(\omega, \varphi)} = \frac{1}{2\pi} \int_{0}^{\infty} E_z(\varphi, t) e^{-j\omega t} \, dt \tag{1c}$$

In this section the actions of the most important elements of the analyzer equipment are summarized.

The direction finder unit derives a "bearing pulse" with a pulse height U_ψ proportional to the apparent azimuth ψ of arrival of the atmospheric.

A narrowband amplifier and rectifier unit derives a d-c pulse U_A, the peak voltage U of which is proportional to $F(\omega, \varphi)$. The angular frequency ω can be selected in the VLF band ($2\pi 5$ kHz to $2\pi 50$ kHz).

Measurements of the spectral amplitude ratio (denoted as SAR in the following) for a pair of frequencies ω_1 and ω_2 are carried out by use of two narrowband amplifiers and a voltage ratio detector. The latter produces a d-c pulse with a height U_R, which is a known function of the ratio $F(\omega_1, \varphi)/F(\omega_2, \varphi)$.

Spectral amplitude and amplitude ratio measurements yield information about the amplitude spectrum $F(\omega, \rho)$. A third mode of operation of the analyzer provides further information related to the phase spectrum $\phi(\omega, \rho)$. It is shown below, that in this way a considerable extension of easily available information about VLF noise has been achieved. The apparatus enables the measurement of a quantity characterizing the dispersion of the received atmospheric spectrum and called the "group delay time difference"(abbreviated as GDD, in what follows). The incoming pulse excites three narrow band circuits tuned to the frequencies

$$\omega_1 = \omega_m - \Delta\omega \ , \quad \omega_m \ , \quad \omega_2 = \omega_m + \Delta\omega$$

which are between 4 kHz and 11 kHz. The circuit responses are combined in such a way that they produce a d-c pulse with the pulse height U_ϕ, which is proportional to the following second order phase difference

$$\Delta^2\phi = \left(\phi(\omega_2) - \phi(\omega_m)\right) - \left(\phi(\omega_m) - \phi(\omega_1)\right) \qquad (2a)$$

This can be approximately expressed by the second order derivative of the phase or the first order derivative of the group delay time with respect to the frequency

$$\Delta^2\phi \cong \frac{\partial^2\phi}{\partial\omega^2}(\Delta\omega)^2 = \frac{\partial t_g}{\partial\omega}(\Delta\omega)^2 = \Delta t_g \, \Delta\omega \qquad (2b)$$

Thus, U_ϕ measures the difference between the group delay times of the spectral components at the frequencies

$$\omega_m - \frac{\Delta\omega}{2} \quad \text{and} \quad \omega_m + \frac{\Delta\omega}{2} \ .$$

The "bearing pulse" U_ψ is fed into the vertical amplifier of an oscilloscope system. The horizontal amplifier can be fed either by the spectral amplitude pulse U_A, or by the pulse U_R measuring the spectral amplitude ratio, or by the pulse U_ϕ measuring the spectral group delay time difference. Every atmospheric produces a short time light spot on the oscilloscope screen, the position of which is uniquely related to its apparent azimuth of arrival and the spectral characteristic selected for being measured.

If the screen is photographed with an exposure time of several minutes, spectral characteristic data of several thousands of atmospherics can be collected and their distribution with respect to the direction can be determined.

3. Considerations on the Physical Significance of
the Observable Spectral Characteristics.

At the present state of our evaluation experience, we use
a simplified form of the waveguide mode theory rather as guide
for presenting the observations than for a quantitative inter-
pretation in terms of propagation models.

3.1 Source Spectrum and Transmission Function

At first, we consider the electromagnetic field excited in
the earth ionosphere waveguide by a CW transmitter, which
radiates the effective power P_r at the angular frequency ω.
The vertical electric component of the field at the distance ρ
has the complex amplitude

$$E_{cw} = \sqrt{\frac{P_r}{1kW}}\; T(\omega, \rho)$$

Here, $T(\omega, \rho)$ is the complex transmission function. If the
radiated signal is a pulse, we have to consider the contri-
bution of the frequency band between $\omega + d\omega/2$ and $\omega - d\omega/2$ to
the radiated power. This contribution is expressed by the com-
plex source spectrum defined by the following equation

$$d\left(\sqrt{\frac{P_r}{1kW}}\right) = g(\omega)\, e^{j\phi_g(\omega)}\, d\omega$$

Thus, the received atmospherics signal is written as

$$E_z(\rho, t) = \int_{-\infty}^{+\infty} g(\omega)\, e^{j\phi_g(\omega)}\, T(\omega,\rho)\, e^{j\omega t}\, d\omega$$

$$(3)$$

3.2 Mode Sum Formulation for the
Transmission Function

For the transmission function the mode sum as given by Wait (Wait and Spies, 1964) is used, simplified by the assumption, that transmitter and receiver are on the ground. Then follows from (11) and (12) of the quoted report by Wait and Spies (1964, p. 4-1) (the factor 300 V is due to the definition of the source spectrum given above)

$$T(\omega,\rho) = \frac{600V}{h}\sqrt{\frac{\lambda}{r_t \sin\frac{\varsigma}{r_t}}}\; e^{-j\frac{\pi}{4}} \sum_{n=1}^{\infty} \Lambda_n e^{-jk\rho\left(1-\frac{1}{2}C_{gn}^2\right)} \tag{4}$$

where h = ionospheric height, defined by Wait and Spies (1964, p. 4-4) in such a way, that it does not depend upon the frequency,

λ = wavelength

k = free space wave number

r_t = terrestrial radius

n = mode order number

$\Lambda_n = |\Lambda_n| e^{j\Phi_{\Lambda n}}$ = complex excitation factor of the nth order mode

The complex parameter C_{gn} follows from the solution of a transcendent mode eigenvalue equation, not discussed here. It may be interpreted to be the cosine of a complex angle of incidence of characteristic waves of the nth order mode to the ground. The corresponding sinus is the complex propagation constant

$$S_{gn} = \sqrt{1-C_{gn}^2} \approx 1 - \frac{1}{2}C_{gn}^2 \tag{5}$$

The propagation constant is related to the phase velocity v_n and attenuation constant A_n of the nth order mode by

$$Re(kS_{gn}) = \frac{\omega}{v_n} \tag{6} \qquad Im(kS_{gn}) = \frac{A_n}{20_{10}\log e} \tag{7}$$

The complex excitation factor, the ratio of the phase velocity
to the free space velocity c and the attenuation parameter
A_n (in dB per 1000 km) are given by the computations of Wait
and Spies (1964, 1965) for frequencies between 8 and 30 kHz,
mode numbers n = 1, 2, and 3, and numerous propagation models.
For frequencies between 5 and 8 kHz, say, we have to try extra-
polating the Wait and Spies-data by means of flat earth propa-
gation models.

Because of the pertinent reference of this paper to the work
of Wait and Spies (1964), a brief description of their propa-
gation models should be repeated: According to Wait and Walters
(1963, 1964) the authors assume the electron density $N_{el}(z)$ to
increase and the collision frequency $\nu_c(z)$ to decrease with the
height z as follows:

$$N_{el}(z) = N_{el}(h)\, e^{b(z-h)} \quad , \quad \nu_c(z) = \nu_c(h)\, e^{-a(z-h)}$$

This results in an exponential increase of the conductivity pa-
rameter ω_r:

$$\omega_r(z) = \frac{3.18 \times 10^9 \, cm^3 \, N_{el}(z)}{\nu_c(z)\, sec^2} = \omega_r(h)\, e^{\beta(z-h)}$$

where $\beta = a + b$. The reference height h is chosen in such a way
that $\omega_r(h) = 2\pi \times 40$ kHz. The ionospheric anisotropy is taken
into account by the parameter

$$\Omega = \frac{\omega_T}{\nu_c(h)}$$

where ω_T is the (angular) gyro frequency. The parameter Ω is ne-
gative for propagation from west towards east, zero for propa-
gation from south to north and vice versa, and positive for pro-
pagation from east towards west.

3.3 The Flat Earth Approximation for Frequencies
of the Lower VLF Band

The sinus S_{gn} of the characteristic angle of incidence of the ground reflection is related to that of a corresponding ionospheric reflection, S_{in}, by

$$S_{gn} = S_{in} \left(1 + \frac{h}{r_t} \right)$$

This can be derived by a simple geometrical consideration. It is convenient to connect the parameters of a curved earth model to those of a flat model with a propagation constant S_n, which is the arithmetic mean between S_{gn} and S_{in}. The propagation constant S_{gn} for the curved model appears then to be the product of the flat earth value S_n and a correction factor:

$$S_{gn} = S_n \left(1 + \frac{h}{2r_t} \right) = \sqrt{1 - C_n^2} \left(1 + \frac{h}{2r_t} \right) \qquad (8)$$

Here, C_n is the solution of the well-known eigenvalue equation for the flat earth wave guide

$$R_g \, R_i \, e^{-j2khC_n} = e^{-j2\pi n} \qquad (9)$$

where R_g and R_i are the reflection coefficients of the ground and the ionosphere, respectively.

For a finite, real ground conductivity σ_g and an ionospheric reflection coefficient of the form

$$R_i \cong - e^{\alpha C} = e^{\alpha_1 C} \, e^{j\alpha_2 C} \, -j\pi$$

the eigenvalues are approx.

$$C_n = \frac{\pi(n - \frac{1}{2})}{kh + j\frac{\alpha}{2}} + j \frac{\sqrt{j \frac{\varepsilon_0 \omega}{\sigma_g}}}{\pi(n - \frac{1}{2})} \qquad (10)$$

The real and imaginary parts α_1 and α_2 of the complex ionospheric parameter α are given by the numerical supplement of the Wait and Spies- report for frequencies between 8 and 30 kHz. By means of (10) the extrapolation of Wait and Spies' attenuation data to frequencies below 8 kHz can be reduced to an extrapolation of the α-values. In this way the influence of extrapolation errors can be kept small. Figure 1 shows values of α_1 and α_2 as given by Wait and Spies for frequencies above 8 kHz and the extrapolated values for 6 kHz used below. The parameters depend upon the height h so slightly, that their values for h = 75 km have been used for all heights. In carrying out the extrapolation, the first four values given by the computations, have been approximated by a cubic parabola.

For extrapolating the phase velocity data, (10) has been used with the gross simplification of neglecting the propagation losses. Then the propagation constant is

$$S_n \cong \sqrt{1 - \frac{\omega_{cn}^2}{\omega^2}} \qquad (11)$$

Here, ω_{cn} is the cutoff frequency of the nth order mode and depends upon the reflection height and the physical nature of the ionospheric reflection. In the range of validity of (10) the ionosphere is nearly a magnetic wall; therefore

$$\omega_{cn} = \frac{(n-\frac{1}{2})\pi c}{h} \qquad (12a)$$

In the lowest ELF range the ionosphere is rather like an electric wall; therefore

$$\omega_{cn} = \frac{n\pi c}{h} \qquad (12b)$$

Between these limiting ranges there is a transition region,
where the angle of incidence of the characteristic waves onto
the ionosphere is in the Brewster-angle range, the reflection
coefficient phase being near -90°. Then is

$$\omega_{cn} \cong \frac{(n-\frac{1}{4})\pi c}{h}$$

(12 c)

No attempt has been made to extrapolate the excitation factor
data to frequencies below 8 kHz, because immediately above
8 kHz they are apparently nearly constant and so small that
no considerable influence upon the measurements may be ex-
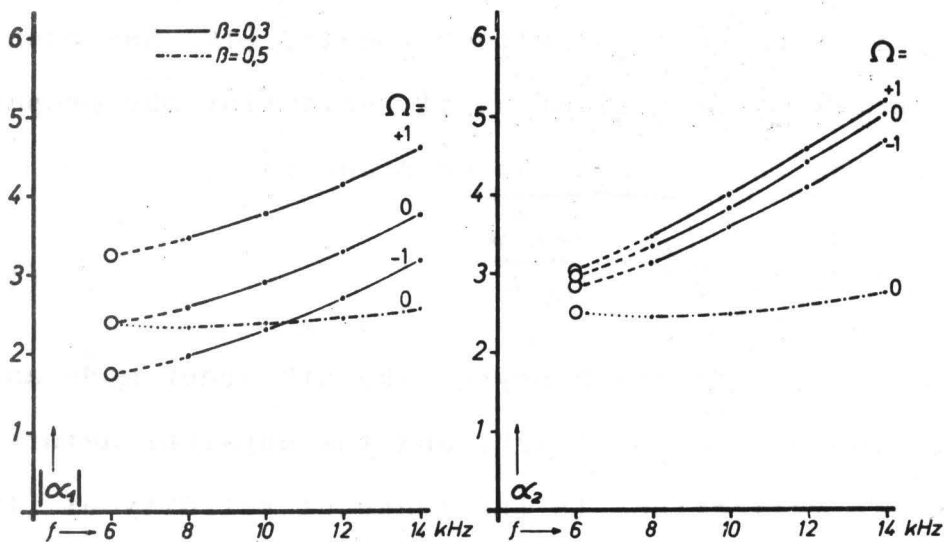pected.

Fig. 1: Real- and imaginary part of the ionospheric
reflection parameter $\alpha = \alpha_1 + j\alpha_2$, plotted as functions
of the frequency for different Wait and Walters-models
at the reference height h = 75 km. Points: Computed data
from Wait and Spies (1965), open circles: Extrapolations.

3.4 Dominant Mode Approximation for the
Transmission Function

The following derivations are simplified by the assumption
that only a single "dominant" mode (of order n = 1) essential-
ly contributes to the received field. In consequence, one can-
not expect observed relations between different spectral para-
meters of every single source to fit theoretically calculated
curves. The collected results, however, of a suffieiently large
number of comparable observations may be expected to scatter
around the results predicted by simplified calculations. If
all higher order modes are neglected, combination of (1), (3),
(4), (6), and (7) gives the interpretation of the received
spectrum in terms of the dominant mode propagation theory (the
angular frequency being replaced by the frequency f):

$$F(f,\varsigma) \cong g(f) \frac{600v}{h} \sqrt{\frac{\lambda}{r_t \sin \frac{\varsigma}{r_t}}} \left| \Lambda_1(f) \right| 10^{-\frac{A_1(f)\varsigma}{20}} \qquad (13a)$$

$$\phi(f,\varsigma) \cong \phi_g(f) + \phi_{\Delta_1}(f) - \frac{\pi}{4} - \frac{2\pi f}{v_1(f)} \varsigma \qquad (13b)$$

The values $A_1(f)$ for several of the well-known ionosphere mo-
dels of Wait and Walters (1963, 1964) and infinitely conduct-
ing earth, as used below for comparison with observations, are
shown by fig. 2a. Above 8 kHz, the attenuations have been taken
from Wait and Spies' numerical work, the values for 6 kHz have
been calculated by flat earth extrapolation, described by the
preceding subsection. The numerical phase velocity data have
been used in a way dealt with by the following subsection.

Fig. 2a:
Attenuation of
the dominant
mode plotted
against the
frequency for
infinitely con
conducting
earth and dif-
ferent Wait
and Walters
models.
Points: Com-
puted by Wait
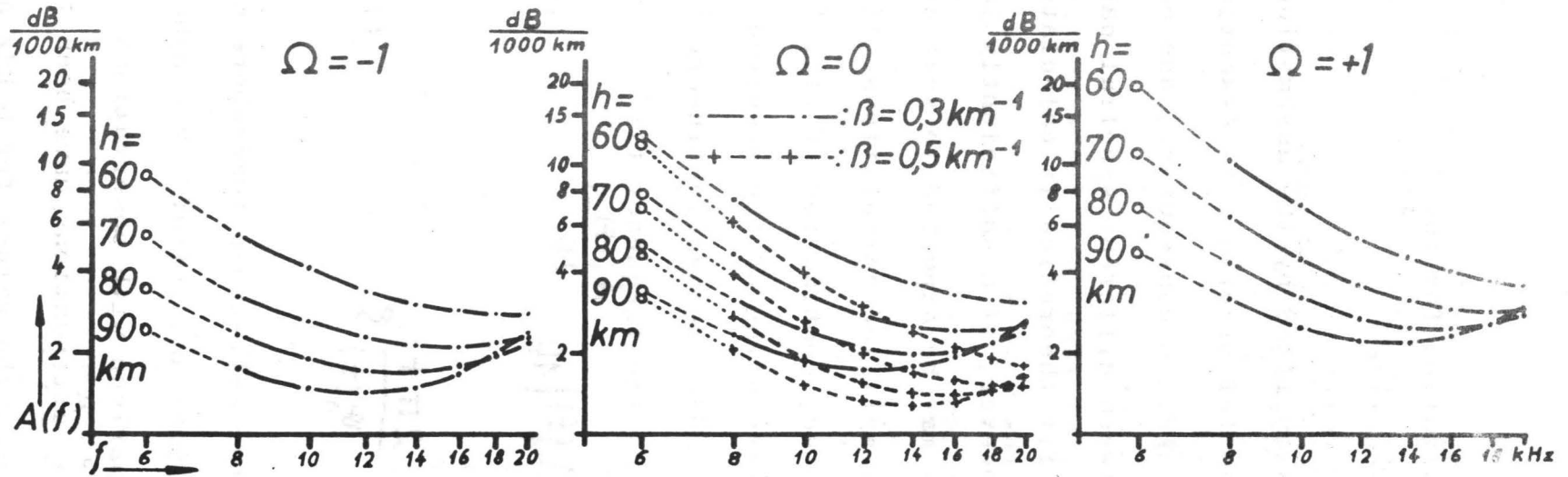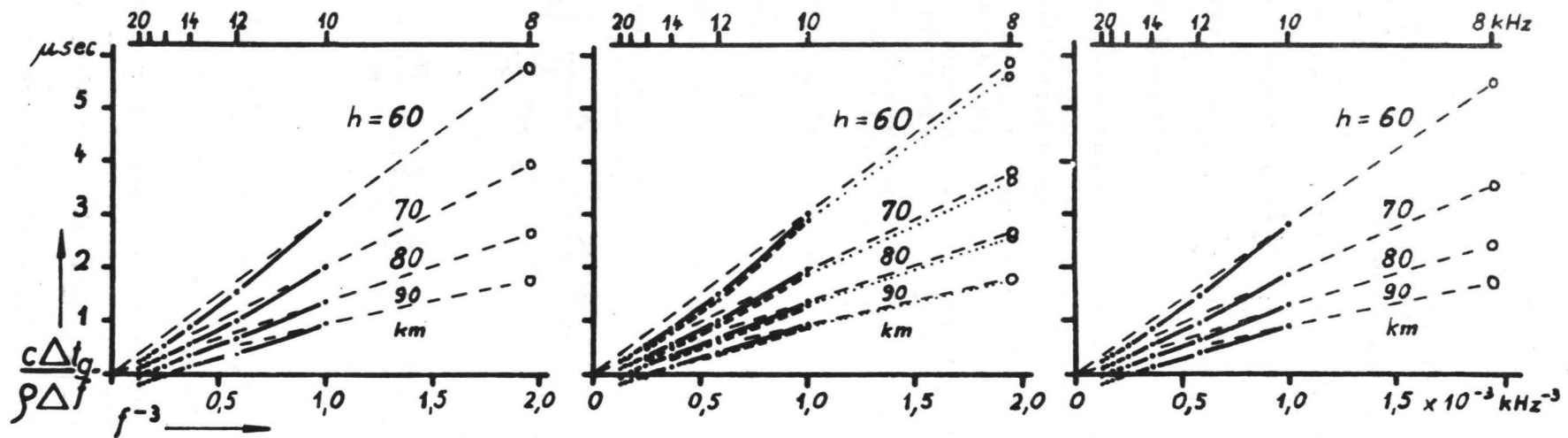and Spies;
Open circles:
Extrapolated

Fig. 2b:
Calculated
ratios bet-
ween normali-
zed GDD's and
ϱ/c.
Points: Deri-
ved from Wait
and Spies
computations;
Open circles:
Extrapolated

3.5 The Physical Significance of the Group
Delay Time Difference Measurements.

The GDD measurements give the second order phase difference
(2a), approximating the derivative of the group delay time with
respect to the frequency (2b). Within the limitations of accu-
racy of the dominant mode approximation (section 3.4), the se-
cond order phase difference (2) can be expressed by the phase
velocity of the mode of order 1 (the angular frequency ω will
be replaced by the frequency f in the following):

$$\left(\Delta^2 \phi\right)_{f_m} = \left(\Delta^2 \phi_g\right)_{f_m} + \left(\Delta^2 \phi_{\Delta 1}\right)_{f_m} - 2\pi g \left(\left(\frac{f_2}{v_1(f_2)} - \frac{f_m}{v_1(f_m)}\right) - \left(\frac{f_m}{v_1(f_m)} - \frac{f_1}{v_1(f_1)}\right)\right) \quad (14)$$

where $f_2 = f_m + \Delta f$ and $f_1 = f_m - \Delta f$. Then the GDD is

$$\left(\Delta t_g\right)_{f_m} = \frac{1}{2\pi \Delta f} \left(\Delta^2 \phi\right)_{f_m} = t_g\left(f_m + \frac{\Delta f}{2}\right) - t_g\left(f_m - \frac{\Delta f}{2}\right) \quad (15)$$

Computed values of $v_1(f)$ are available for the frequencies
$f = 8, 10, 12, ..., 30$ kHz; thus, the second order phase dif-
ferences can be calculated for the middle frequencies $f_m =$
$10, 12, ..., 28$ kHz.

Measurements of the GDD are experienced to be feasible for
medium frequencies below 10 kHz. Values of f_m adopted for mea-
surement programs were 8, 7, and 6 kHz, the frequency distance
Δf being 2, 1.4 and 1 kHz, respectively. Thus, observed GDDs
will be compared with calculated ones, which have been extra-
polated from those following from the Wait and Spies- phase
velocity data.

Using the loss free flat earth approximation for the propagation constant in the lower VLF band((8) and (11), n = 1), we get

$$D(f) = \frac{\partial t_g}{\partial f} \cong \left(1 + \frac{h}{2r_t}\right)\frac{f_{c1}^2}{f^3}\left(1 - \frac{f_{c1}^2}{f^2}\right)^{-\frac{3}{2}}\frac{\varsigma}{c} \cong \left(1 + \frac{h}{2r_t}\right)\frac{f_{c1}^2}{f^3}\frac{\varsigma}{c} \quad (16a)$$

Here, f_{c1} is the cutoff frequency of the first order mode (see (12a, b, and c)). This may be written as

$$D(f) \cong \frac{c^2}{\xi^2\, h^2\, f^3}\frac{\varsigma}{c} \quad (16b)$$

where the factor ξ has been introduced to take into account both the curvature of the earth and the physical character of the ionospheric reflection. From (12) we get

$$\xi = 4\left(1 + \frac{h}{2r_t}\right)^{-\frac{1}{2}} \qquad \text{if the ionosphere is a magnetic wall, (17a)}$$

$$\xi = 2\left(1 + \frac{h}{2r_t}\right)^{-\frac{1}{2}} \qquad \text{if the ionosphere is an electric " , (17b)}$$

$$\xi = \frac{8}{3}\left(1 + \frac{h}{2r_t}\right)^{-\frac{1}{2}} \qquad \text{if the ionosphere reflection is of}$$
$$\text{Brewster-angle type.} \quad (17c)$$

For lossfree propagation with a magnetic wall ionosphere and middle frequencies above 8 kHz, equation (16b) has been compared with earlier curved earth computations of Spies and Wait (1961). It has been found , that the proportionality to f^{-3} is valid also for curved waveguide models, but the factor ξ is essentially more decreased by the curvature of the earth, than predicted by (17).

For the D-layer models of the Wait and Spies-report used in this paper, the proportionality factor between the normalized GDD, $\Delta t_g/\Delta f$, and ς/c has been calculated for $f_m = 10, 12, \ldots, 20$ kHz using (14), and neglecting the contributions of the source spectrum and the excitation factor phase.

The results, plotted as functions of f_m^{-3}, are shown by fig.2b. Apparently the proportionality between the GDD and f_m^{-3} is a useful approximation even for realistic curved earth models, and for $f_m = 8$ kHz the straight line extrapolations shown by fig. 2b have been used below.

The f^{-3}-extrapolations are further justified by the experience, that the observed GDDs, plotted against f_m^{-3}, fit straight lines within a satisfactory approximation, as described by a companion paper (Heydt, Frisius, in preparation).

According to the proportionality of the GDD to h^{-2}, as predicted by (16), the calculated normalized GDDs for $f_m = 10$ kHz have been plotted against h^{-2} for two isotropic models (fig.3). The GDD proves to be approx. proportional to $(h^{-2} - (140 \text{ km})^{-2})$. This relationship can be tested, if sources showing sufficiently large GDD-values can be observed over periods of at least 24 hours. Such observations have been carried out by Harth (Volland, Heydt, and Harth, 1967), but in general it is difficult to find appropriate sources.

Of greatest practical interest is the proportionality of the GDD to the distance ρ, predicted by (16). If any relation of such simplicity would be valid, the GDD measurement would permit the localization of atmospheric sources by means of a single station. Considerable attention has therefore been paid to the problem of experimentally determining the relation between the source distance and the observed GDDs. To this end, numerous spheric location messages of the British Meteorological Office have been confronted to GDDs of sources, observed by means of network of three atmospherics analyzers (Heydt, Frisius, Volland, and Harth, 1968). The success was

unsatisfactory because for sources with small GDD-values (i.e. small distances) the dominant mode approximation is not valid. For sources showing large GDD-values, however, no information on their location has been available. To overcome this difficulty, attempts have been made to use cloud photographs of the ESSA-satellite (Volland, Heydt, and Harth, 1968). The problem, however, to identify certain cloud configurations with atmospherics sources needs still discussion, apparently.

Therefore, we have to conclude, that this problem cannot be solved without carrying out really comparable measurements at sufficiently separated observing sites.
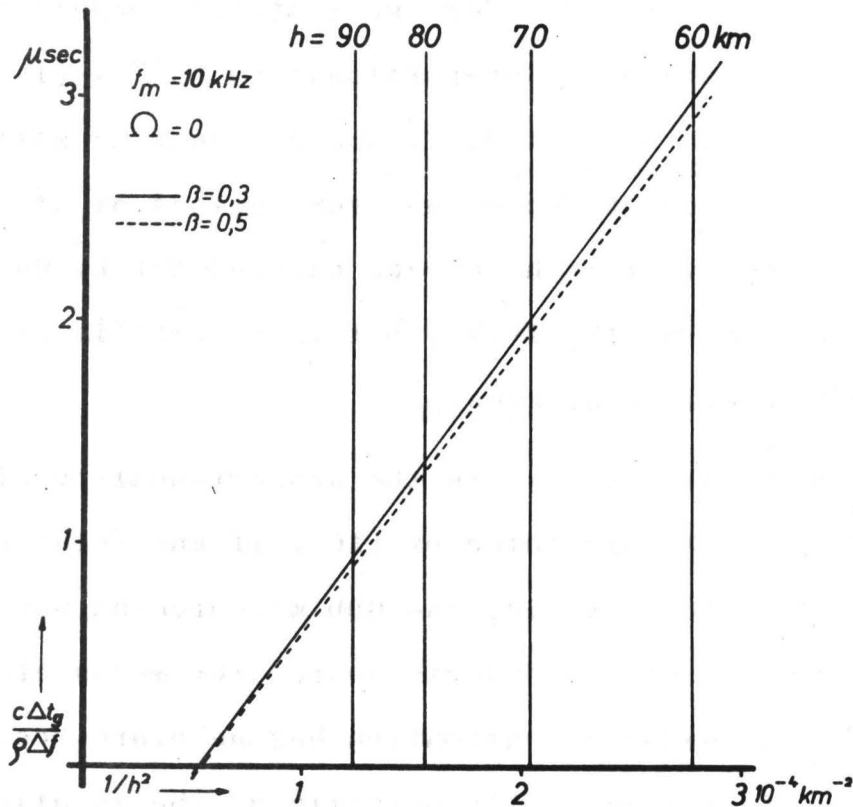

Fig. 3: Calculated ratios between normalized group delay time differences and ϱ/c for the middle frequency 10 kHz, plotted against h^{-2} (ϱ = propagation distance, h = reference height of the Wait and Walters-models).

3.6 Physical Significance of the Spectral
Amplitude Ratio Measurements

For the SAR between two frequencies f_1 and f_2 we get the
following interpretation from (13a):

$$20 \log \frac{F(f_1, \varrho)}{F(f_2, \varrho)} \cong 20 \log \frac{g(f_1)\, h(f_2)\, \sqrt{\lambda_1}\, |\Lambda_1(f_1)|}{g(f_2)\, h(f_1)\, \sqrt{\lambda}\, |\Lambda_1(f_1)|} - \left(A_1(f_1) - A_1(f_2)\right)\varrho \quad (18)$$

This means: If the results of the SAR measurements (expressed
in dB) could be plotted as a function of ϱ, one should get a
straight line with a slope, indicating the attenuation para-
meter difference $(A_1(f_1) - A_1(f_2))$. The ionosphere height h is
defined by Wait and Spies (1964, p. 4-4) in such a way, that
it does not depend upon the frequency. Thus, the intercept of
the straight line with the ordinate axis $(\varrho = 0)$ would contain
two unknown quantities: The ratio of the source spectrum values
and of the amplitudes of the excitation factor at the frequen-
cies f_1 and f_2.

The direct experimental verification of (18) was affected by
the same difficulties as described at the end of the preceding
subsection.

4. Presentation of Observations

Because of the unsolved problem of reliable source localization, it is not possible to plot the observed spectral characteristics as functions of the distance. Valuable information, however, can still be achieved, if instead of the distance, one of the observed GDDs is taken for the independent variable, e.g. that with f_m = 8 kHz. This quantity has been experienced to give well readable measuring photos and is expected to linearly depend upon the distance (14 and 16). This idea is the basis of the following presentation of spectral data of all sources, that could be observed during a four week's period. The material is subdivided with respect to both daytime and direction of arrival. To this end, the azimuth has been divided into eight 45°-sectors (denoted N, NE, E, ... and so on), and the observations of eight measuring times of every day (at 01^{oo}, 04^{oo}, 07^{oo}, ... and so on) have been selected for being presented.

May 12th – June 8th, 1967

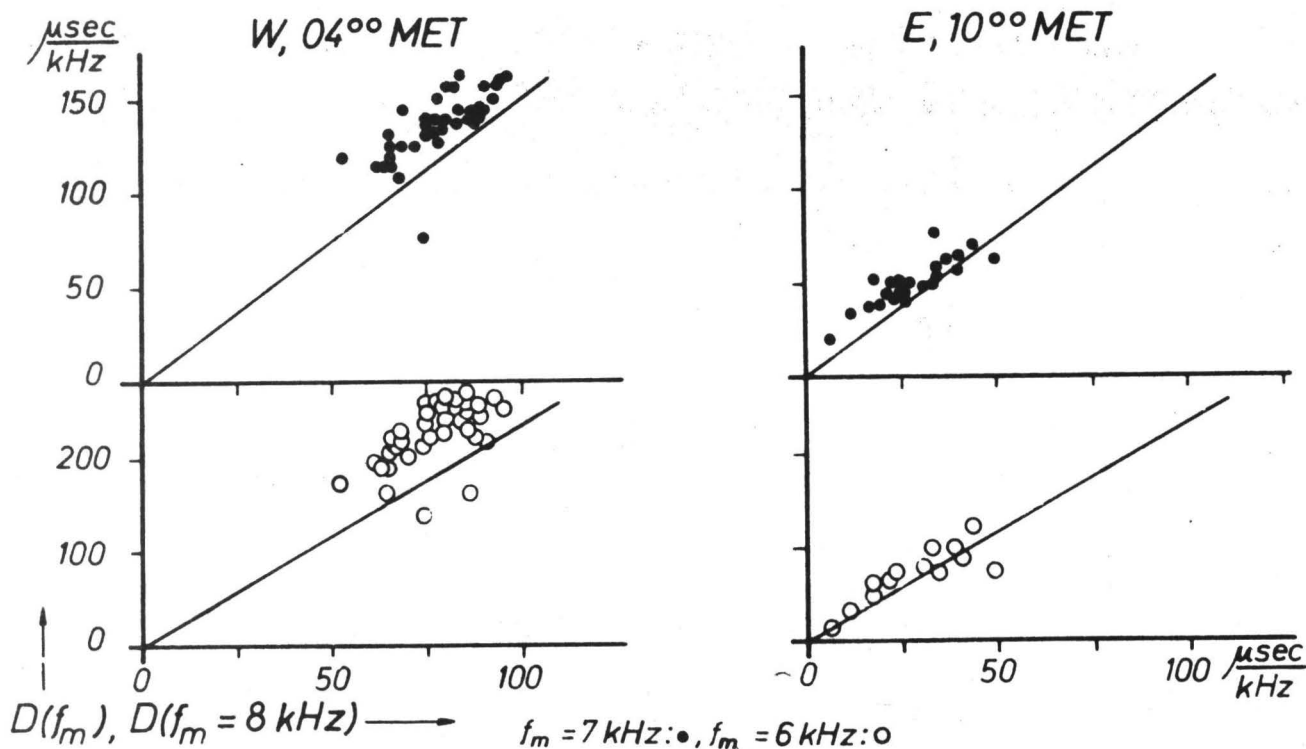$D(f_m), D(f_m = 8\ kHz)$ ⟶ f_m = 7 kHz:•, f_m = 6 kHz:o

Fig. 4: Correlations between normalized GDD's at different middle frequencies (straight lines: theoretical).

4.1 Observed Relation between Group Delay Time
Differences at Different Middle Frequencies

If (16b) is valid, then the normalized GDD at a middle fre-
quency f_{m2} depends upon that at another middle frequency f_{m1}
by

$$D(f_{m2}) = \frac{\xi^2(f_{m1})\, h^2(f_{m1})\, f_{m1}^3}{\xi^2(f_{m2})\, h^2(f_{m2})\, f_{m2}^3} D(f_{m1}) \qquad (19)$$

If h and ξ do not significantly depend upon f_m, then $D(f_{m2})$ is
expected to be a linear function of $D(f_{m1})$ with the slope
(f_{m1}^3 / f_{m2}^3).

In fig. 4, data are shown of sources observed during the
four weeks' period

(a) in the sector west at the measuring time 04^{00} (night),

(b) in the sector east at the measuring time 10^{00} (day).

The observed GDDs at f_{m2} = 7 and 6 kHz respectively are corre-
lated to those at f_{m1} = 8 kHz. Straight lines with the slope
(f_{m1}^3 / f_{m2}^3) have been drawn too, and it can be seen that most
of the observed sources gave points, which lie reasonably near
to them. Apparently, most of the $D(f_{m2})$-values are a little
larger than predicted by the straight lines. This can be ex-
plained either by a decrease of ξ (compare (17)) or by a de-
crease of h with decreasing frequency.

A complete survey on all sources observed during the period
under consideration is given by fig. 5. Some remarkable points
should be noticed:

Fig. 5:
Survey on all
GDD's observed
during a peri-
od of 4 weeks,
(compare fig.
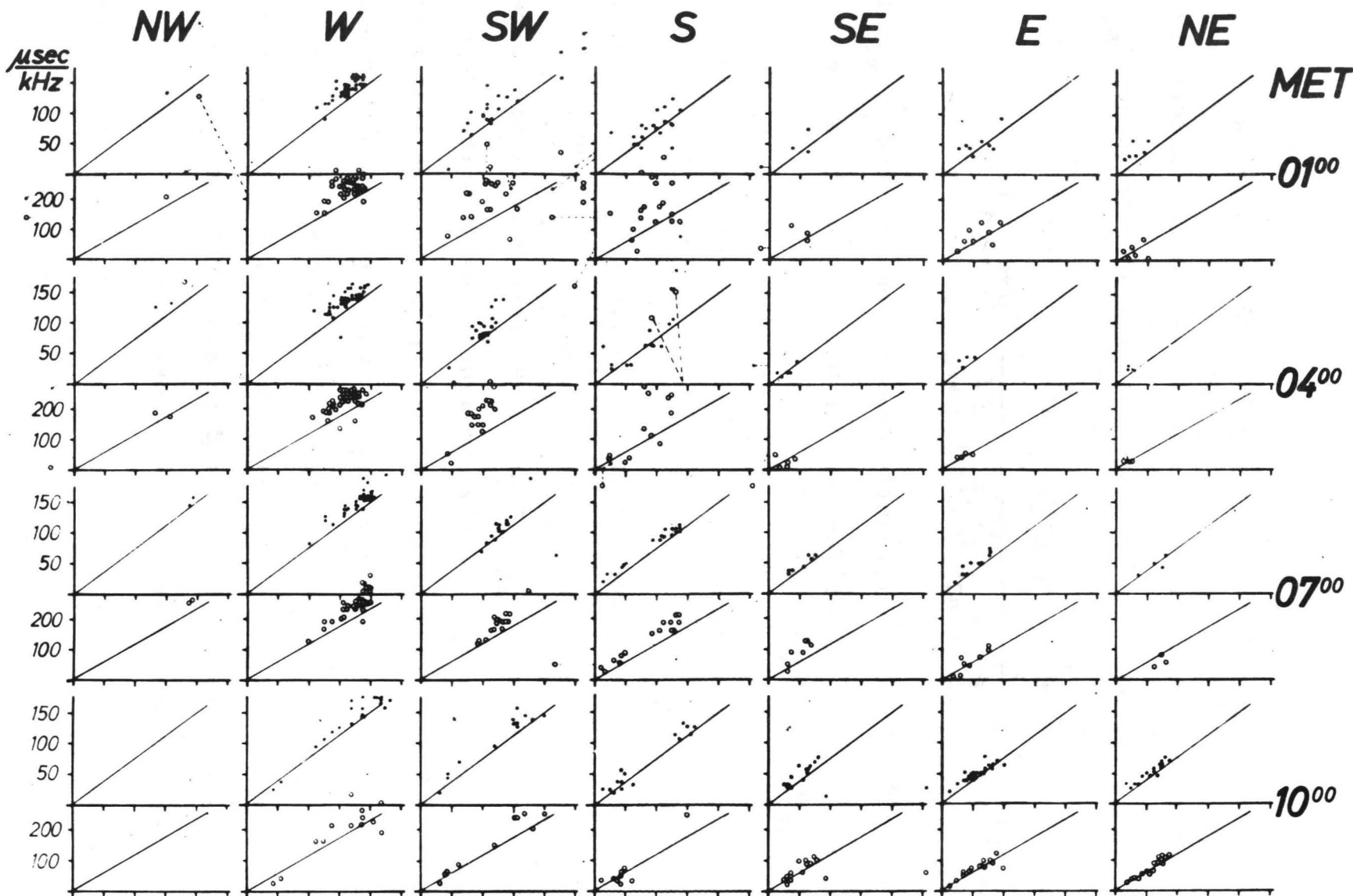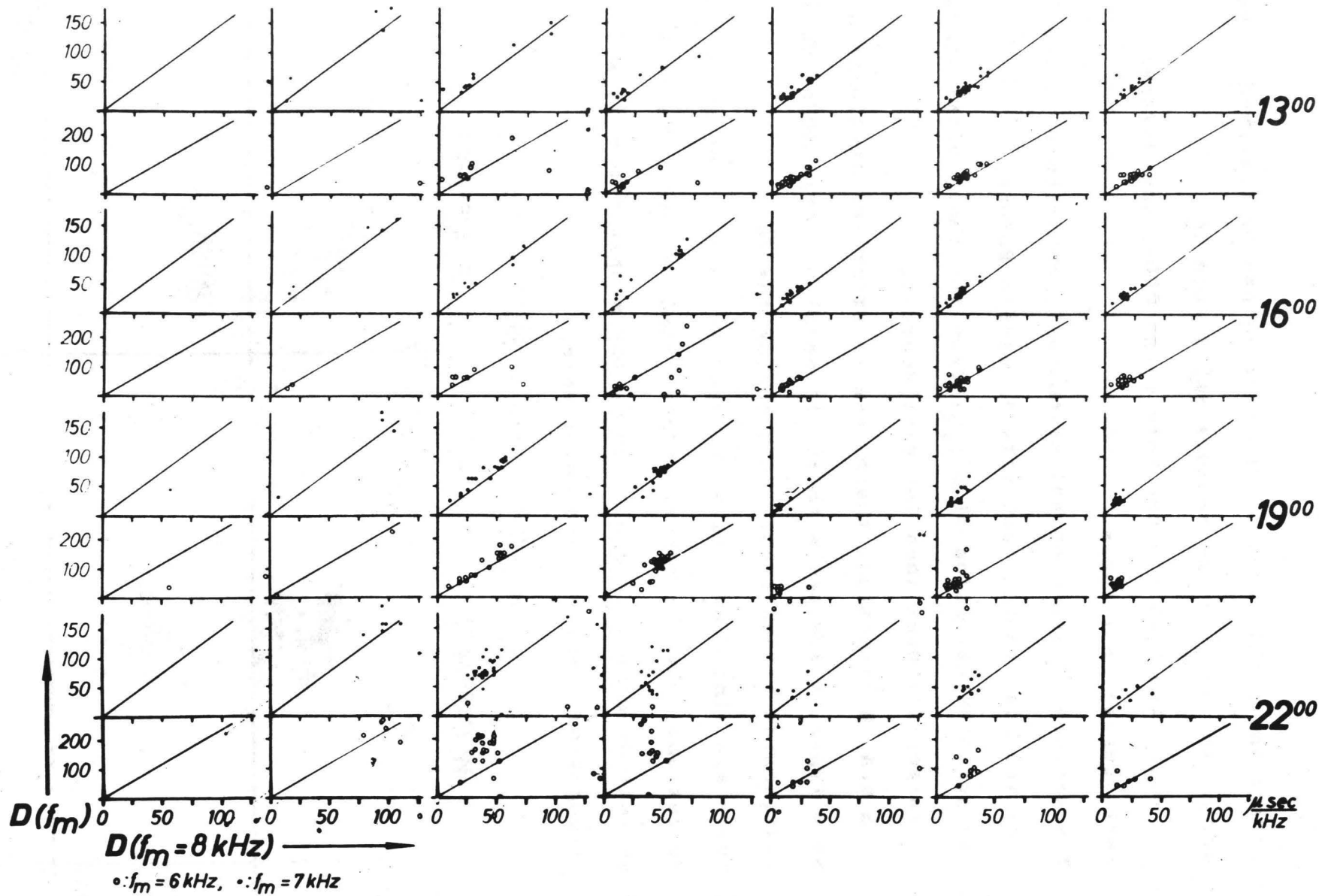4).

May, 12ᵗʰ – June, 8ᵗʰ,1967

Fig. 5
(continued)

$D(f_m)$

$D(f_m = 8\,kHz)$ ⟶

$\circ : f_m = 6\,kHz, \quad \bullet : f_m = 7\,kHz$

13^{00}

16^{00}

19^{00}

22^{00}

$\dfrac{\mu\,sec}{kHz}$

1) During the night, most of the sources can be observed at west, during the day, on the sectors SE, E, and NE.

2) The nighttime west sources have large GDDs, the daytime east sources small ones.

3) The sectors NW and N do not essentially contribute to the observed atmospherics activity in middle Europe.

4) The positive deviation of $D(f_{m2})$ from the theoretical lines is larger for west than for east sources.

5) In S and SW direction, there seem to exist two distinguishable types of sources with either small or large GDDs. This distinction is observable only during the day.

6) There are single sources with negative GDDs and/or gross deviations from the behaviour predicted by (16b). These observations cannot be explained by the simple dominant mode propagation theory we are using here.
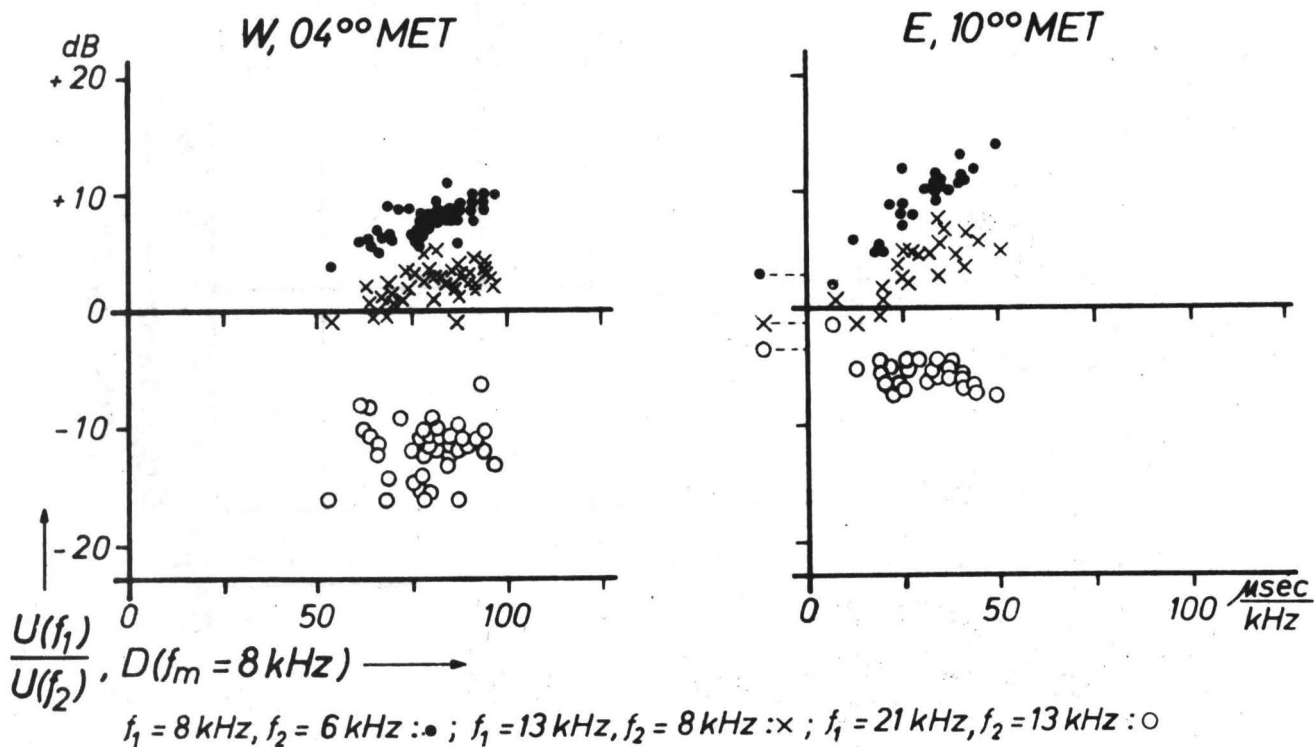
May 12th – June 8th, 1967

$f_1 = 8\,kHz, f_2 = 6\,kHz : \bullet$; $f_1 = 13\,kHz, f_2 = 8\,kHz : \times$; $f_1 = 21\,kHz, f_2 = 13\,kHz : \circ$

Fig. 6: Correlations between SAR's for different frequency pairs and the normalized GDD at 8 kHz.

4.2 Observed Relations Between Spectral Amplitude
Ratios and Group Delay Time Differences

Let us replace the distance ϱ on the right hand term of (18) by the normalized GDD at f_m = 8 kHz, using (16). It is easily to be seen, that the relation between SARs and GDDs may be expected to be linear. This is at least not contradicting the experience, as to be seen by fig. 6. Here, SAR measurements of the same sources as in fig. 4 are correlated to the corresponding GDD measurements (for f_m = 8 kHz). For the SAR measurements, three pairs of frequency have been used. The first pair, 8 and 6 kHz, is in that frequency range, where the received atmospherics amplitude spectrum is experienced to increase with the frequency (Taylor, 1967). This is shown by positive values of the SAR.

The second pair, 13 and 8 kHz, is near to the well-known maximum of the VLF radio noise spectrum. Apparently, most of the SARs are still positive, but essentially smaller than for the first pair.

A third pair of frequency, 21 and 23 kHz, is in a range where the spectrum is decreasing with increasing frequency. The SARs are therefore negative.

As in the preceding section, it is possible to calculate theoretical SAR-GDD-correlation lines, which provide an insight into the physical significance of the observed correlations. To this end, the attenuation data computed by Wait and Spies (1964) for the mentioned frequencies (with flat earth extrapolation for 6 kHz, fig. 2a) have been inserted into (18). In replacing the ϱ scale by a D(8 kHz)-scale, the extrapolated values for $\Delta t_g \times c/\Delta f \times \varrho$ following from fig. 2b have been used.
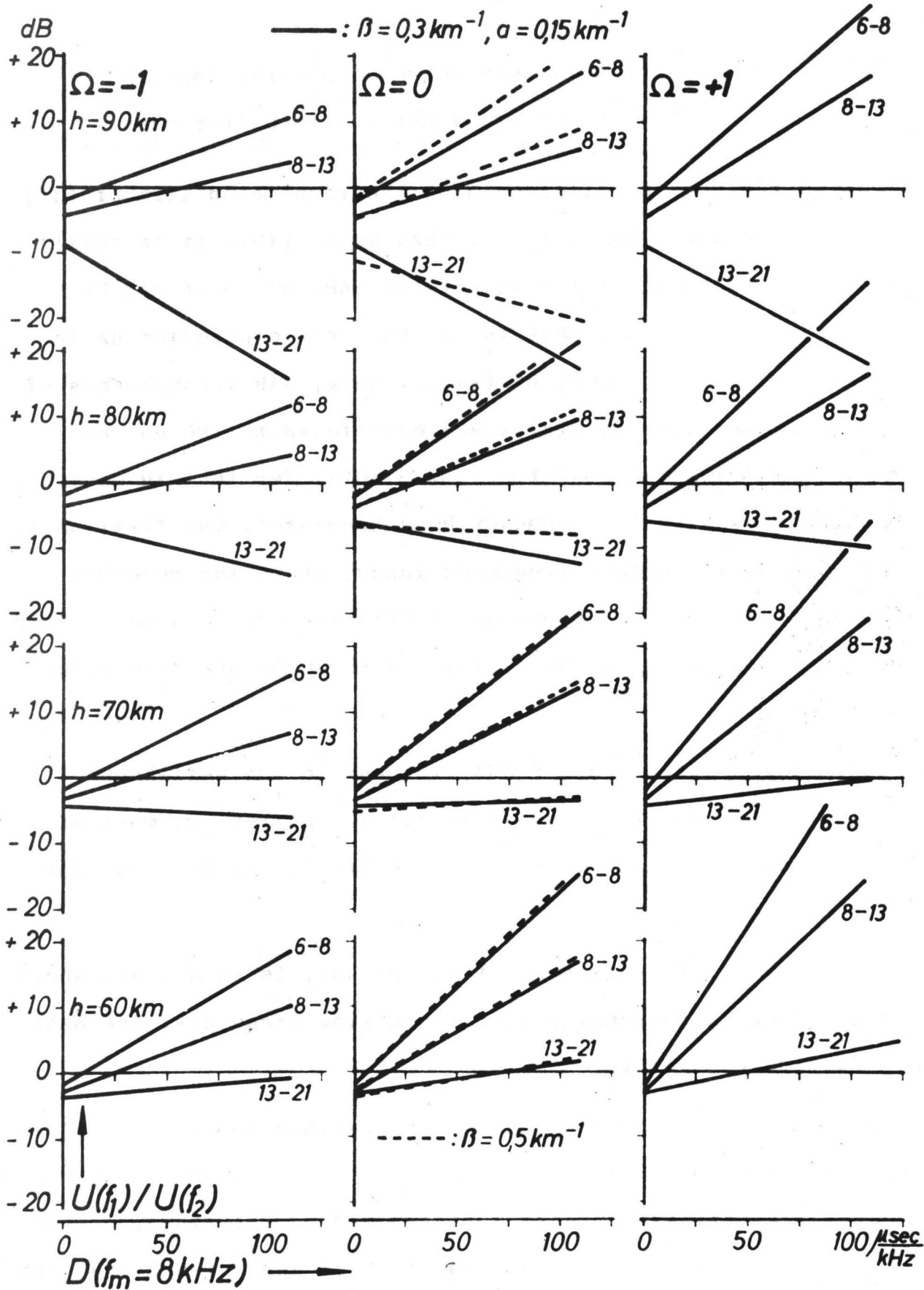
Fig. 7: Correlations between SAR's for the same frequency pairs as in fig. 6, and the normalized GDD at 8 kHz, calculated by use of the theoretical attenuation and GDD values shown by fig. 2.

The calculated correlation lines for the Wait and Spies-
model data, compiled by figures 2a and b, are shown by fig. 7.
They are arranged in such a way that they can easily be com-
pared with the observed data, compiled by fig. 8 for the same
sources as in fig. 5. The reader may compare the west obser-
vations with the theoretical lines for the anisotropy parameter
Ω = -1, the south observations with the lines for Ω = 0, and
the East observations with the lines for Ω = +1; further the
01^{00}, 04^{00}, and the 22^{00}-observations with the theoretical lines
for h = 80 and 90 km, the 10^{00}, 13^{00}, and the 16^{00}-observations
with the lines for h = 60 and 70 km. The following characteri-
stics are to be found in both figures:

1) The slopes of the 6 – 8 – lines are larger than those of the
   8 – 13 – lines, the latter larger than those of the 13 – 21 –
   lines. This is due to the steep increase of the propagation
   attenuation towards ELF frequencies and the broad attenua-
   tion minimum near 12 kHz at night and near 18 kHz by day.

2) The slopes of the SAR-lines are larger for E – W than for
   W – E propagation. This is due to the well-known nonreci-
   procity between W – E and E – W propagation.

3) The intercepts of the 8 – 13 – lines with the D(8 kHz)-axis
   are nearer to the zero for E – W than for W – E propagation.

4) The intercepts of the 13 – 21 – lines with the ordinate axis
   are remarkably more negative at night than by day. This is
   an effect of the steep decrease of the excitation factor
   for frequencies above 15 kHz, say, and for nighttime condi-
   tions. For daytime conditions the range of steep decrease
   of the excitation factor trends towards frequencies larger
   than 30 kHz.

Fig. 8:
Survey om all
SAR's obser-
ved during a
period of 4
weeks and cor-
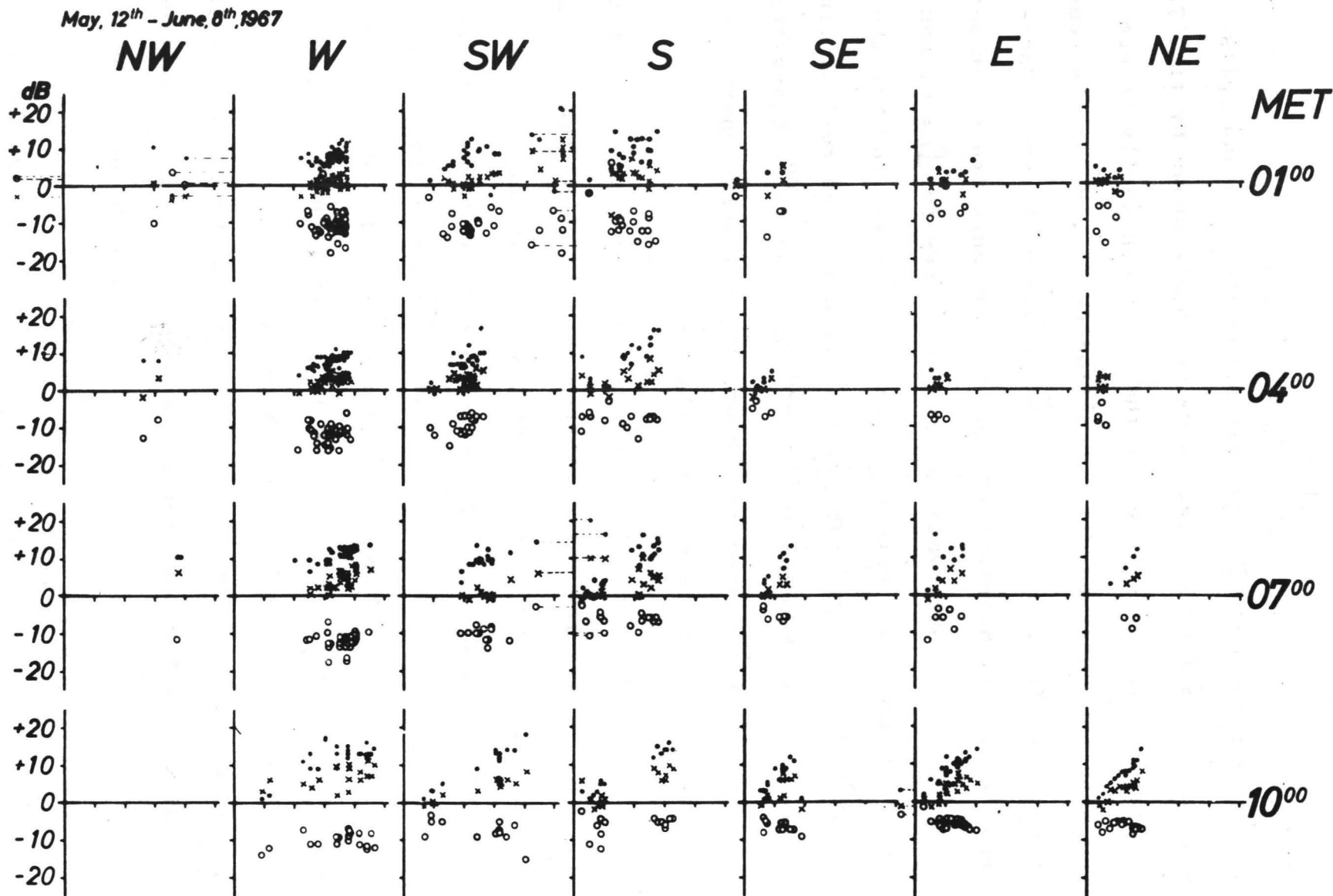related to
the normali-
zed GDD's at
8 kHz, as in
fig. 5

May, 12th – June, 8th, 1967

NW   W   SW   S   SE   E   NE

MET

Fig. 8
(continued)

$U(t_1)/U(t_2)$

$D(f_m = 8\,kHz) \longrightarrow$

$\bullet: f_1 = 8, f_2 = 6\,kHz;$ $\times: f_1 = 13, f_2 = 8\,kHz;$ $\circ: f_1 = 21, f_2 = 13\,kHz$
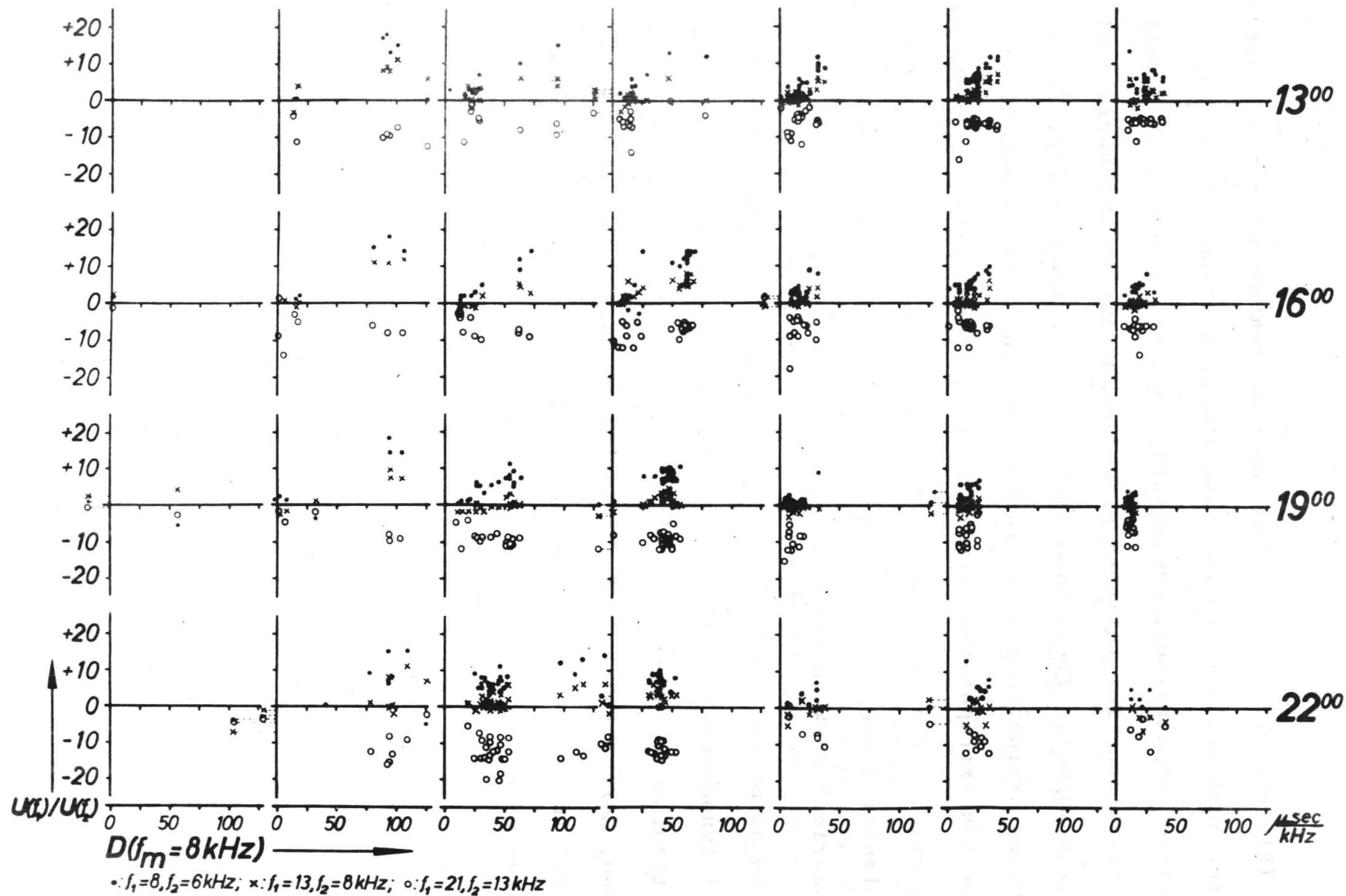
13^{00} 16^{00} 19^{00} 22^{00}

This comparison shows the basic agreement between atmospherics analyzer observations and the predictions of the Wait and Spies- computations. One should remember, however, that only computations for infinite ground conductivity and horizontal earth magnetic field have been used in preparing fig. 7. For future evaluations it is further desirable to eliminate the unknown extrapolation errors from the theoretical predictions, especially the loss free - flat earth approximation for the calculated GDDs. This can be done as soon as extensions of the numerical work to ELF frequencies are available.

No attention has been paid here to the influence of horizontal inhomogenities of the terrestrial waveguide on the propagation. Such influences can be observed (Heydt, Frisius, Volland, Harth, 1968), and a description appropriate for theoretical interpretation is being developed and will be communicated later.

5. Concluding Remarks

If the mentioned shortcomings of the theoretical inter/pretation can be eliminated, the atmospherics analyzer may be expected to be a powerful tool for investigating both, the propagation characteristics of the earth ionosphere wave guide and the distribution of the VLF atmospherics activity with respect to time and geographical position.

The most effective improvement of the method, however, would be achieved, if the outstanding problem of the localization of the atmospherics sources could be solved by coordinated measurements at widely spaced stations. This is considerably facilitated by the automatic operation of the analyzer device, which has been experienced to work perfectly during a test period of 14 months. Thus, the localization problem is apparently of purely organizational nature.

References

Heydt, G. (1967). Peilanlagen zur Messung von spektralen Ampli-
    tudenverteilungen, Amplitudenverhältnissen und Grup-
    penlaufzeitdifferenzen von Atmospherics. Techn. Ber.
    No. 90 of the Heinrich-Hertz-Institut für Schwingungs-
    forschung, Berlin-Charlottenburg.

Heydt, G., J. Frisius, H. Volland, W. Harth (1967). Beobachtung
    entfernter Gewitterzentren mit dem Atmospherics-Ana-
    lysator des Heinrich-Hertz-Institutes. Kleinheubacher
    Berichte, 12, 103-110.

Heydt, G. and J. Frisius (1968). A New Technique to Observe
    Spectral Parameters of the VLF Radio Noise as Functions
    of the Azimuth. (In preparation).

Spies, K. P. and J. R. Wait (1961). Mode Calculations for VLF
    Propagation in the Earth Ionosphere Wave Guide.
    NBS, Techn. Bote No. 114.

Taylor, W. L. (1967). VLF Transmissions Loss Calculated from
    Spectral Analyses of Atmospherics.
    Radio Sci. 2 (New Ser.), 139-145.

Volland, H., G. Heydt, W. Harth (1967). The Statistical Measure-
    ment of Spectral Amplitudes and Phases of Atmospherics
    in the VLF Range. XIII-th Symposium of the AGARD-EPC
    on Phase and Frequency Instability in Electromagnetic
    Wave Propagation. (In print).

Wait, J. R. and L. C. Walters (1963). Reflection of VLF Radio
    Waves from an Inhomogeneous Ionosphere, Parts I, II,
    and III. J. Res. NBS 67D (Radio Prop.) 361 - 367,
    509 - 523, 747 - 752.

Wait, J. R. and L. C. Walters (1964). Reflection of Electro-
    magnetic Waves from a Lossy Magnetoplasma. J. Res.
    NBS 68D (Radio Sci.) 95 - 101.

Wait, J. R. and K. P. Spies (1964). Characteristics of the
    Earth-Ionosphere Waveguide for VLF Radio Waves.
    NBS, Techn. Note No. 300.

Wait, J. R. and K. P. Spies (1965). Numerical Supplement to
    NBS Techn. Note No. 300.